




Towards adiabatic-connection interpolation model with broader applicability

Lucian A. Constantin ¹, Szymon Śmiga ², and Fabio Della Sala ^{3,1,*}

¹*Institute for Microelectronics and Microsystems (CNR-IMM), Via Monteroni, Campus Unisalento, 73100 Lecce, Italy*

²*Institute of Physics, Faculty of Physics, Astronomy, and Informatics, Nicolaus Copernicus University in Toruń, ul. Grudziądzka 5, 87-100 Toruń, Poland*

³*Center for Biomolecular Nanotechnologies, Istituto Italiano di Tecnologia, Via Barsanti 14, 73010 Arnesano (LE), Italy*



(Received 11 March 2024; revised 23 May 2024; accepted 24 May 2024; published 14 June 2024)

The adiabatic connection integrand interpolation (ACII) method represents a general path for calculating correlation energies in electronic systems within the density functional theory. ACII functionals include both exact-exchange and the second-order correlation energy, as well as an interpolating function toward the strictly correlated electron (SCE) regime. Several interpolating functions have been proposed in the last years targeting different properties, yet an accurate ACII approach with broad applicability is still missing. Recently, we have proposed an ACII functional that was made accurate for the three-dimensional (3D) uniform electron gas as well as for model metal clusters. In this paper we present an ACII functional (named genISI2), which is very accurate for both three-dimensional (3D) and two-dimensional (2D) uniform electron gases and for the quasi-2D infinite-barrier model, where most of the exchange-correlation functionals fail badly, as well as for strongly correlated two-electrons systems. Using the exact-exchange Kohn-Sham orbitals, we have also assessed the genISI2 for various molecular systems, showing a superior performance with respect to the other ACII methods for total energies, atomization energies, and ionization potentials. The genISI2 functional can thus find application in a broad range of systems and properties.

DOI: [10.1103/PhysRevB.109.235129](https://doi.org/10.1103/PhysRevB.109.235129)

I. INTRODUCTION

Nowadays, the ground-state Kohn-Sham (KS) density functional theory (DFT) [1,2] is widely used in electronic structure calculations of finite and extended systems [3–7], providing an adequate ratio between the accuracy and computational time. The basic DFT variable is the ground-state electronic density $n(\mathbf{r})$, which implicitly determines all the ground-state properties of the electronic system [8,9]. In the KS-DFT, $n(\mathbf{r})$ is found by solving the Euler equation via one-particle orbitals $\{\phi_{i,\sigma}(\mathbf{r})\}$, such that the noninteracting kinetic energy functional is treated exactly as $T_s[n(\mathbf{r})] = \langle \Phi_n^{\min} | \hat{T} | \Phi_n^{\min} \rangle = \int d\mathbf{r} \sum_{i,\sigma}^{\text{occ}} |\nabla \phi_{i,\sigma}|^2 / 2$, where Φ_n^{\min} is the Slater determinant build with KS one-particle orbitals $\{\phi_{i,\sigma}(\mathbf{r})\}$, that yields the density $n(\mathbf{r})$ and minimizes the expectation value of the kinetic energy operator $\langle \hat{T} \rangle$. Thus, only the exchange-correlation (XC) energy functional $E_{xc}[n(\mathbf{r})]$ must be approximated. We recall that the XC energy functional should describe the electron-electron interactions beyond the classical Hartree energy $U[n] = (1/2) \int d\mathbf{r} \int d\mathbf{r}' n(\mathbf{r})n(\mathbf{r}')/|\mathbf{r} - \mathbf{r}'|$.

An elegant (and exact in principle) definition of the XC functional uses the adiabatic connection (AC) method [10–16],

$$E_{xc}[n] = \int_0^1 d\alpha W_{xc,\alpha}[n],$$

$$W_{xc,\alpha}[n] = \langle \Psi_n^{\min,\alpha} | \hat{V}_{ee} | \Psi_n^{\min,\alpha} \rangle - U[n], \quad (1)$$

where \hat{V}_{ee} is the Coulomb repulsion operator, and $\Psi_n^{\min,\alpha}$ is the antisymmetric wave function that yields the density $n(\mathbf{r})$ and minimizes the expectation value $\langle \hat{T} + \alpha \hat{V}_{ee} \rangle$, with $\alpha \geq 0$ being the coupling constant (also known as interaction strength).

There are many XC functionals constructed in the framework of the AC method, including accurate hybrid functionals [8,15,17–19] and the most sophisticated fifth-rung functionals [20] (which uses the unoccupied orbitals in the functional definition) such as the random phase approximation (RPA) [21–23] and double-hybrid (DH) functionals [24].

In the fifth rung are also included the functionals investigated in this paper, i.e., the one based on a $W_{xc,\alpha}[n]$ model [25–51], which interpolates between the weak- ($\alpha \rightarrow 0$) and strong- ($\alpha \rightarrow \infty$) interaction limits, and that we refer to as “adiabatic connection integrand interpolation” (ACII).

We recall that the asymptotic behaviors of $W_{xc,\alpha}[n]$ are known exactly [26,31,52,53]

$$W_{xc,\alpha \rightarrow 0}[n] = W_0[n] + W'_0[n]\alpha + \dots$$

$$+ W_0^{(m)}[n]\alpha^m + \dots, \quad (2)$$

$$W_{xc,\alpha \rightarrow \infty}[n] = W_\infty[n] + W'_\infty[n]\alpha^{-1/2}$$

$$+ W_\infty^{(2)}[n]\alpha^{-3/2} + \dots \quad (3)$$

*fabio.dellasala@imm.cnr.it

Here, $W_0[n] = E_x[n]$ is the exact DFT exchange functional, $W'_0[n] = 2E_c^{GL2}[n]$, and $W_0^{(m)}[n] = (m+1)E_c^{GL_{m+1}}[n]$, where GL indicated the Görling-Levy perturbation theory [52,54,55]. Usually, only the GL2 correlation (E_c^{GL2}) is included in the ACII functionals. In some schemes, the GL2 terms are approximated with a semilocal functional [13,47,50,51]: in this way, however, the whole functional does not belong anymore to the fifth rung.

In the strong-interaction limits the strictly correlated electron (SCE) approach [56–58] becomes exact. On the other hand, the SCE method becomes computationally very demanding, especially for larger systems, such that usually $W_\infty[n]$ and $W'_\infty[n]$ are approximated using generalized gradient approximation (GGA) or meta-GGA formulas [27,45,48,51].

One of the first and most known ACII functional is interaction strength interpolation (ISI) [26]. In the last years, different approaches and investigations have been presented [39,42,43,45–48,50], including those based on the Hartree-Fock (HF) density [59–63]. Efficient implementation of ACII methods is also available in public quantum-chemistry codes [64].

After the α integration the total XC energy of ACII functionals becomes a nonlinear function (\mathcal{F}) of the E_x , E_c^{GL2} , W_∞ , and W'_∞ ingredients,

$$E_{xc}[n] = \mathcal{F}(E_x, E_c^{GL2}, W_\infty, W'_\infty). \quad (4)$$

Equation (4) thus resembles DH functionals [24]: however, ACII employs a nonlinear dependence from the GL2 term and does not diverge for systems with vanishing gaps [39,47,64], which is a clear superiority with respect to DH approaches.

Recently, we have proposed the UEG-ISI functional [50], an ACII functional (valid in the limit of $E_c^{GL2} \rightarrow -\infty$) that gives an improved description of the three-dimensional (3D) uniform electron gas (UEG). Then, the UEG-ISI has been supplemented by a term that depends on E_c^{GL2} , finally yielding the genISI functional [50], with good performance for jellium clusters and atoms.

In this paper, we construct the genISI2 XC functional as a revision of the one proposed in Ref. [50], fulfilling the negativity constraint of the correlation energy ($E_c \leq 0$) for any possible values of the ingredients W_0 , W'_0 , W_∞ , and W'_∞ . Both the genISI and genISI2 functionals recover UEG-ISI in the limit of $E_c^{GL2} \rightarrow -\infty$.

We assess the genISI and genISI2 functionals for various systems such as the two-dimensional (2D) UEG, the quasi-2D infinite-barrier model (IBM), the Hooke's atom and the dissociation of the spin-restricted H_2 molecule, which are very hard tests for XC functionals:

The 2D UEG is a paradigm for 2D electronic systems [65], and the 2D local density approximation (LDA) XC functional yields already quite a good accuracy for the total energy of many 2D systems [66]. However, most of 3D XC functionals fail badly for 2D UEG, and only few high-level methods, such as the inhomogeneous Singwi-Tosi-Land-Sjölander (ISTLS) can accurately describe the 2D UEG [67,68].

The quasi-2D IBM [69–74], which is a severe test for the dimensional crossover from 3D to 2D, is poorly described both at the RPA and the semilocal (GGA and meta-GGA)

levels of theory, e.g., see Refs. [45,72]. For example, the popular Perdew–Burke–Ernzerhof (PBE) GGA [75] and the Tao-Perdew-Staroverov-Scuseria (TPSS) [76] meta-GGA XC functionals fail badly for this test.

The Hooke's atom [77–84], also named harmonium, represents two interacting electrons in an isotropic harmonic potential of frequency ω ($\omega = \sqrt{\kappa}$, where κ is the force constant). At small values of ω , the electrons are strongly correlated, and at large frequencies, they are tightly bound [85]. Because ACII formulas interpolate between the weak- and strong-correlation limits, this is a very important test.

The H_2 dissociation curve using a spin-restricted formalism, which is a widely studied prototype of a strongly correlated system [38–41,86–94]. While most of XC functionals gives the correct energy at the equilibrium distance, only the most advanced functionals can correctly describe the static correlation at infinite distance [41,89,91,95,96].

In addition, we considered the more conventional molecular systems, investigating the accuracy for total energies, atomization energies, and ionization potentials. The performances of genISI and genISI2 are then discussed in comparison with the other well-known ACII functionals.

The paper is organized as follows: In Sec. II, we overview the genISI and present the construction of genISI2 XC functional. Computational details are described in Sec. III, while in Sec. IV, we report the results for various systems. Finally, in Sec. V, we summarize our conclusions.

II. THEORY

A. Overview of the genISI exchange-correlation functional

In the UEG-ISI functional [50] the AC integrand is

$$W_{xc,\alpha}^{UEG-ISI}[n] = W_\infty[n] + \frac{b(2 + c\alpha + 2d\sqrt{1 + c\alpha})}{2\sqrt{1 + c\alpha}(d + \sqrt{1 + c\alpha})^2}, \quad (5)$$

where

$$\begin{aligned} b &= b[n] = (W_0[n] - W_\infty[n])(1 + d) \geq 0, \\ c &= c[n] = b[n]^2 / (4W_\infty'^2[n]) \geq 0, \\ d &= 3.5. \end{aligned} \quad (6)$$

The parameter d has been optimized, minimizing the error for the correlation energy per particle (ϵ_c) of the 3D UEG. For small α we have

$$W_{xc,\alpha}^{UEG-ISI}[n] \rightarrow W_0[n] - s[n]\alpha + \dots \quad (7)$$

with

$$s[n] = \frac{1 + d}{4} \frac{(W_0[n] - W_\infty[n])^3}{W_\infty'^2[n]} \geq 0. \quad (8)$$

Note that there are no exact conditions for the coefficient $s[n]$, as the UEG-ISI functional is built for metallic systems, in which $E_c^{GL2} = -\infty$, see the discussion in Ref. [50]. The UEG-ISI XC energy is

$$\begin{aligned} E_{xc}^{UEG-ISI}[n] &= \int_0^1 d\alpha W_{xc,\alpha}^{UEG-ISI}[n] \\ &= W_\infty[n] + \frac{b[n]}{d + \sqrt{1 + c[n]}}. \end{aligned} \quad (9)$$

The genISI functional adds a E_c^{GL2} dependent term to UEG-ISI; it has the following expression for the AC integrand:

$$W_{xc,\alpha}^{genISI}[n] = W_{xc,\alpha}^{UEG-ISI}[n] + \frac{A[n]\alpha}{(1 + m r[n]p[n]\alpha)^3}, \quad (10)$$

with

$$p[n] = W_0'[n]/W_0[n] \geq 0, \quad A[n] = W_0'[n] + s[n],$$

$$r[n] = \left(\frac{W_0[n]}{W_\infty[n]} \right)^3 \geq 0, \quad m = 18.0. \quad (11)$$

The parameter m has been obtained by fitting to the correlation energy of harmonium with force constant $\kappa = 1/4$ [45,77]. The genISI functional has been constructed so that for small α it recovers the exact expansion,

$$W_{xc,\alpha}[n] \rightarrow W_0[n] + (2E_c^{GL2})\alpha + \dots \quad (12)$$

Integrating over α , we obtain a simple analytical expression for the genISI XC energy,

$$E_{xc}^{genISI}[n] = E_{xc}^{UEG-ISI}[n] + \frac{A[n]}{2(m r[n]p[n] + 1)^2}. \quad (13)$$

B. The genISI2 functional

For the genISI2 functional, we consider the following expression:

$$W_{xc,\alpha}^{genISI2} = W_{xc,\alpha}^{UEG-ISI} + W_{xc,\alpha}^{a1} + W_{xc,\alpha}^{a2},$$

$$W_{xc,\alpha}^{a1} = \frac{W_0'[n]\alpha}{(1 + l_1 r[n]p[n]\alpha)^3} \leq 0,$$

$$W_{xc,\alpha}^{a2} = \frac{-W_{xc,\alpha}^{UEG-ISI}[n] + W_0[n]}{(1 + l_2 r[n]p[n]\alpha)^3} \geq 0. \quad (14)$$

For small α the genISI2 behaves as

$$W_{xc,\alpha}^{genISI2} \rightarrow W_0[n] + \left(2 + \frac{6l_2 W_0[n]^2 (W_{xc,\alpha=0}^{UEG-ISI}[n] - W_0[n])}{W_\infty[n]^3} \right) \times \alpha E_c^{GL2} + \dots \quad (15)$$

Thus, using Eq. (7), we have that genISI2 recovers the exact limit in Eq. (12).

The genISI2 XC energy

$$E_{xc}^{genISI2}[n] = \int_0^1 d\alpha W_{xc,\alpha}^{genISI2}[n], \quad (16)$$

does not have a simple analytical expression (as genISI). Still, the integral over the coupling constant can be numerically computed with high efficiency and accuracy (e.g., using a Gaussian quadrature with only 16 points).

The genISI2 functional recovers all the exact conditions fulfilled by revISI [30], LB [31], genISI, and additionally, the genISI2 correlation energy is always negative. This is not the case for the genISI functional. We mention that for all the studied systems, we have found the correct behavior of genISI (i.e., $E_c^{genISI} \leq 0$); however in principle, E_c^{genISI} can be

TABLE I. Exact (or almost exact) ACII ingredients (in E_h) and negative of correlations energies ($-E_c$ in mE_h) from several ACII functionals, computed for the harmonium with force constant $\kappa = 1/4$, the two-electron exponential density $[n(r) = 2\exp(-2r)/\pi]$, Exp.], and the He, Be, and Ne atoms. The exact values are from Ref. [50] and references therein. In the last column, we show the MARE (in %) of each method. Best ACII results are in boldface.

	Harm.	Exp.	He	Be	Ne	
W_∞^{SCE}	-0.743 ^a	-0.910 ^c	-1.500 ^c	-4.021 ^h	-20.035 ^h	
W_∞^{SCE}	0.208 ^a	0.293 ^c	0.621 ^g	2.590 ^g	22.0 ^g	
W_0	-0.515 ^b	-0.625 ^c	-1.024 ^f	-2.673 ^f	-12.078 ⁱ	
W_0'	-0.101 ^b	-0.093 ^d	-0.095 ^e	-0.246 ^f	-0.948 ⁱ	
						MARE (%)
SPL	35.9	35.6	39.9	104.0	428.8	7.1
LB	38.5	37.8	41.6	108.1	436.8	5.8
ISI	36.6	36.4	40.5	102.4	414.3	5.1
revISI	37.0	36.9	40.8	101.7	409.3	4.1
genISI	39.6	37.4	39.3	106.5	415.7	5.8
genISI2	37.2	38.0	42.3	97.2	391.9	1.8
Exact	38.5	37.3	42.1	94.4	391.0	

^afrom Ref. [31].

^bfrom Table IV of Ref. [29].

^cfrom Table I of Ref. [25].

^dfrom Table I of Ref. [101].

^eReference [102].

^ffor Table II and Table IV of Ref. [16], using accurate density.

^gfrom Table 1 of Ref. [30].

^hfrom Table I of Ref. [103], using accurate density.

ⁱcomputed in this work at the CCSD(T)/unc-aug-cc-pV6Z density.

positive, probably outside of the physical range of W_0 , W_0' , W_∞ and W_∞' ingredients. In fact, the quantity $A[n]$ can be positive for small values of E_c^{GL2} (see Appendix for further details).

Moreover, by construction,

$$\lim_{W_0' \rightarrow 0} E_c^{genISI2} = 0, \quad (17)$$

a condition not satisfied by genISI, see Eq. (13). We recall that W_0' vanishes not only for any one-electron systems (where genISI is also exact because of $W_0 = W_\infty$), but also for a perfect insulator (where genISI will fail), an interesting model system used in the DFT and solid-state physics development [97,98]. Note that the correlation energy of the jellium-with-gap model vanishes in the limit of infinite band gap energy [99,100], such that Eq. (17) remains valid in this case.

Finally, the parameters l_1 and l_2 were found from the minimization of the mean absolute relative error (MARE) of several small spherical systems, as described in the following subsection.

C. Small systems with accurate ingredients

For few spherical systems (harmonium with force constant $\kappa = 1/4$, the two-electron exponential density $[n(r) = 2\exp(-2r)/\pi]$, and the He, Be, Ne), the ingredients (W_0 , W_0' , W_∞^{SCE} , and $W_\infty'^{SCE}$) are known (almost) exactly from literature (see Table I). For the neon atom, we recomputed W_0 and W_0' using the the coupled-cluster single double and perturbative

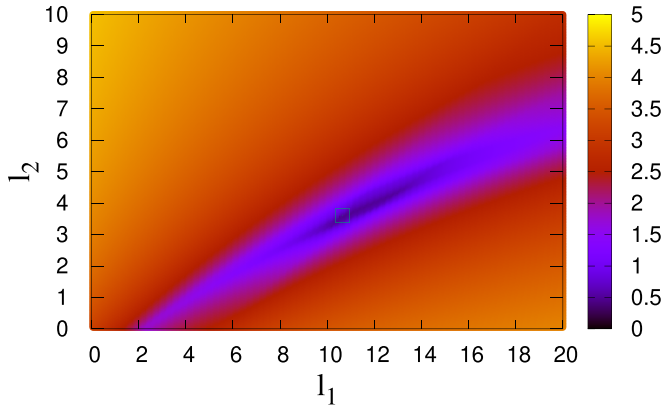


FIG. 1. $\log[\text{MARE}(l_1, l_2)]$ (in %) of correlation energies computed for the systems of Table I, from the genISI2 expression of Eq. (16), as a function of the l_1 and l_2 parameters. The minimum of the $\log[\text{MARE}(l_1, l_2)]$ is at $l_1 = 10.65$ and $l_2 = 3.6$ (shown with an empty square), i.e., the parameters used in the genISI2 functional.

triple [CCSD(T)] density and inversion technique (see Sec. III for details).

Figure 1 reports the $\text{MARE}(l_1, l_2)$ of the correlation energies of these systems, computed with the genISI2 expression, as a function of the l_1 and l_2 parameters. The minimum error is found at $l_1 = 10.65$ and $l_2 = 3.6$, which we use to define the genISI2 functional. Basically, the same parameters are obtained if we consider the absolute error per electron instead of the absolute relative error.

In Table I, we show the correlation energies of these systems, computed from several ACII functionals. The genISI2 functional gives the best MARE ($\approx 2\%$) showing that the genISI2 functional form is flexible enough to describe the correlation in these systems.

In Fig. 2, we show a comparison between UEG-ISI, ISI, genISI, and genISI2 for adiabatic connection correlation integrand $W_{c,\alpha} = W_{xc,\alpha} - W_0$ of harmonium ($\kappa = 1/4$) and Ne atom. We observe that both genISI and genISI2 curves are smooth and realistic, being close to the exact result. On the other hand, the UEG-ISI integrand does not have the right slope at $\alpha = 0$, showing a strong underestimation. We recall that the area under the curves for $0 \leq \alpha \leq 1$ represents the correlation energy $E_c = \int_0^1 d\alpha W_{c,\alpha}$. However, we mention that for both atoms, the genISI2 gives the best performance, being better than ISI and genISI. Noting that the CCSD(T) correlation energy of the reference curve of the lower panel of Fig. 2 is about 14 mE_h bigger than the benchmark reference (see Table I), we may even expect that $W_{\alpha,c}^{\text{genISI2}}$ is the most accurate shown result for the Ne atom.

III. COMPUTATIONAL DETAILS

A. (quasi-)2d systems

The calculations for the quasi-2D IBM in Sec. IV A use exact orbitals and densities [69]. Thus W_0 and W'_0 ingredients are exactly computed [104], while for the strong-interaction limit ingredients W_∞ and W'_∞ we use (at any quantum well thickness) accurate interpolations between the 2D and 3D limits, as explained in detail in Sec. IV A. Note that for $W_\infty(L_{\max})$

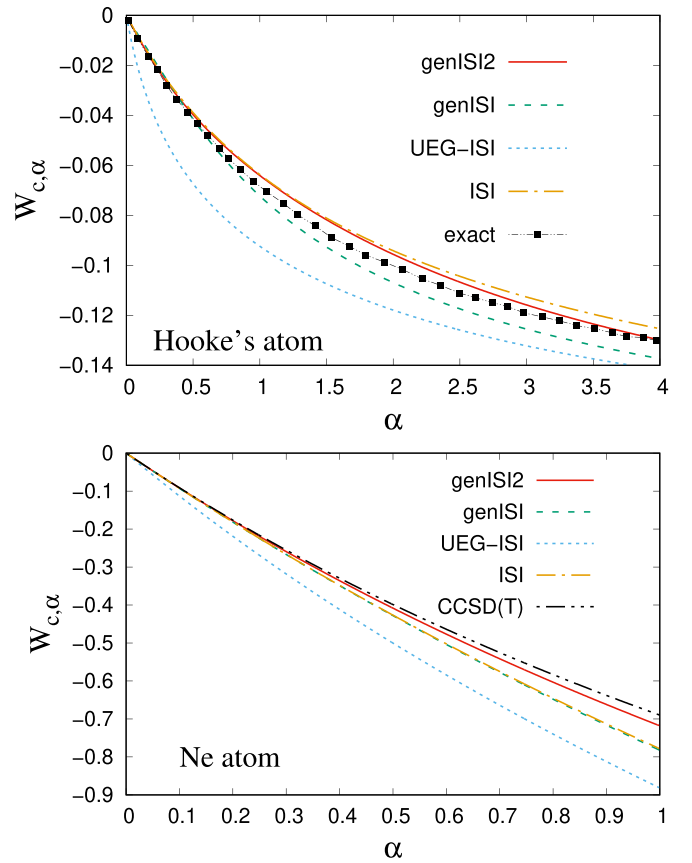


FIG. 2. The adiabatic connection correlation integrand $W_{c,\alpha} = W_{xc,\alpha} - W_0$, for harmonium ($\kappa = 1/4$) (upper panel) and for the Ne atom (lower panel). The harmonium exact curve is from Ref. [29] and the Ne atom CCSD(T) reference (with uncontracted aug-cc-pCVQZ basis set) is from Ref. [94]. We use the exact/accurate (SCE) ingredients shown in Table I.

and $W'_\infty(L_{\max})$ we use the meta-GGA functional of Ref. [105] and Ref. [27], respectively. For the 2D uniform electron gas in Sec. IV B, we use the exact ingredients.

B. Atoms and molecules

All calculations have been performed with a locally modified version of ACES II [106] program. All ACII results have been obtained in a post-self-consistent-field (SCF) fashion, using as a reference OEPx SCF converged quantities (i.e., orbitals, orbital energies, and densities). As in our previous studies [47,48,107,108] to solve OEPx equations, we have employed the finite-basis set procedure from Ref. [109]. The harmonium point-charge-plus-continuum (PC) model (hPC) [48] was used in all calculations to evaluate the W_∞ and W'_∞ .

In particular, we have investigated:

(i) Harmonium: We have performed calculations for various values of $\omega \in [0.03, 1000]$ in the harmonium model [110] using the computational setup and an even-tempered Gaussian basis set (up to f angular momentum functions) from Ref. [111].

(ii) Total energies: The total energies (reported in Table V) have been calculated for the systems listed in Table I of Ref. [112], using an identical computational setup.

(iii) Atomization energies: AE6 [113,114] atomization energies listed in Table VI. These calculations have been performed using uncontracted cc-pVTZ basis sets of Dunning [115] without counterpoise corrections for basis set superposition error (BSSE). The results have been corrected for size-consistency error according to Ref. [43]. (Note, however, that this correction is very small for atomization energies.)

(iv) Vertical ionization potentials: 32 vertical ionization potentials (VIP) [116] computed as the energy difference between the neutral and the ionic species [117]. The computational setup, namely basis sets and geometries (in the case of molecules), is identical as in Ref. [116].

For total energies, atomization energies, and ionization potentials, we used, as reference data, the CCSD(T) [118] results obtained in the same basis set to make a comparison on the same footing and to reduce basis set related errors.

C. Accurate reference for atomic systems

To compute the reference W_0 , W_∞ , W'_∞ , and E_c^{GL2} values reported in Tables I and III, one needs to obtain accurate KS occupied and unoccupied orbitals from which E_c^{GL2} can be evaluated. To this end, we have considered the densities from full configuration interaction (FCI), in the case of harmonium and He atoms, and CCSD(T), for Ne atom. The KS potential is then obtained using the Wu-Yang (WY) [119] inversion procedure. All calculations have been performed in a locally modified PySCF [120] program together with *KS-pies* package [121] for the WY method. In all calculation, the lambda regularization parameter [122] was set to 10^{-5} and the Fermi-Amaldi guide potential was used to correct the asymptotic behavior of the XC potentials. We used the uncontracted aug-cc-pV6Z [123] basis set for He and Ne atoms and for harmonium the basis set from Ref. [111].

IV. RESULTS

In this section, we validate the accuracy of the genISI2 functional for the quasi-2D IBM model (see Sec. IV A) for the two-dimensional electron gas (see Sec. IV B) and for finite systems (see Sec. IV C).

A. quasi-2d IBM

Let us consider the quasi-2D IBM quantum well of thickness L in the z direction [69–74]. The true 2D uniform electron gas limit is recovered by shrinking the z coordinate, keeping fixed the total number of electrons per unit area (n^{2D}). The quasi-2D regime is obtained when $L \leq \sqrt{3/2}\pi r_s^{2D} = L_{\max}$ [69], being equivalent to a nonuniform scaling in one dimension [i.e., $n_\lambda^z(x, y, z) = \lambda n(x, y, \lambda z)$, with $\lambda = L_{\max}/L$]. The 3D density of this quasi-2D system is

$$n(z) = \frac{2}{L\pi (r_s^{2D})^2} \sin^2(\pi z/L). \quad (18)$$

We perform similar calculations to those reported in Fig. 6 of Ref. [69]. Thus, we use the following ingredients for the

ACII methods:

$$W_0(L)/N = E_x(L)/N, \quad (19)$$

where $E_x(L)/N$ is the exact exchange per particle calculated with exact orbitals for the quasi-2D IBM of thickness $L \leq L_{\max}$. We recall that most semilocal exchange functionals fail badly for the quasi-2D IBM system [70,74], diverging in the limit $L \rightarrow 0$. Note that

$$W_0(0)/N = E_x(0)/N = -4 \frac{\sqrt{2}}{3\pi} \frac{1}{r_s^{2D}}, \quad (20)$$

is the exchange energy per particle of the 2D uniform electron gas.

For $W_\infty(L)/N$ we use the physically motivated interpolation proposed in Ref. [69],

$$\frac{W_\infty(L)}{N} = \left[\frac{W_\infty(0)}{W_0(0)} \left(1 - \frac{L}{L_{\max}}\right) + \frac{W_\infty(L_{\max})}{W_0(L_{\max})} \frac{L}{L_{\max}} \right] \frac{W_0(L)}{N}, \quad (21)$$

where

$$W_\infty(0)/N = W_\infty^{2D}/N = \left(\frac{8}{3\pi} - 2 \right) \frac{1}{r_s^{2D}}, \quad (22)$$

and $W_\infty(L_{\max})/N$ has been computed using the W_∞^{TPSS} of Eq. (37) of Ref. [105], that is one of the most accurate models for W_∞ of 3D electronic systems.

On the other hand, for $W'_\infty(L)/N$ we use the simplest interpolation

$$\frac{W'_\infty(L)}{N} = \frac{W'_\infty(0)}{N} \left(1 - \frac{L}{L_{\max}}\right) + \frac{W'_\infty(L_{\max})}{N} \frac{L}{L_{\max}}, \quad (23)$$

where

$$W'_\infty(0)/N = W_\infty'^{2D}/N = \frac{1}{2(r_s^{2D})^{3/2}}, \quad (24)$$

and $W'_\infty(L_{\max})/N$ has been computed using $W_\infty'^{MGGA}$ of Eq. (D16) of Ref. [27].

Finally, the $W'_0(L)/N$ is known exactly

$$W'_0(L)/N = 2E_c^{GL2}(L)/N, \quad (25)$$

where $E_c^{GL2}(L)/N$ is given by Eq. (45) of Ref. [104]. We observe that for 2D UEG, $E_c^{GL2}(0)/N = -0.1925$ Ha, being independent on r_s^{2D} and finite, in contrast to the 3D UEG case where $E_c^{GL2}/N \rightarrow -\infty$. In fact, in the high-density limit of 2D UEG ($r_s^{2D} \rightarrow 0$), $\epsilon_c \rightarrow E_c^{GL2}(0)/N = -0.1925 E_h$ [65].

In Fig. 3, we show all these ingredients for $r_s^{2D} = 1, 3$, and 5, respectively. At high densities (for $r_s^{2D} = 1$), we observe that $W_\infty/N \leq E_x/N \leq W'_0/N \leq 0 \leq W'_\infty/N$, while at low densities (for $r_s^{2D} = 5$), the pattern is different $W'_0/N \leq W_\infty/N \leq E_x/N \leq 0 \leq W'_\infty/N$. In the figure, we also show ϵ_c^{LDA} , for a better comparison with the other ingredients. Note that, $\epsilon_c^{LDA} \propto \ln(r_s)$ has a logarithmic divergence at $L \rightarrow 0$, where the 3D bulk parameter is going to vanish ($r_s \rightarrow 0$) due to the 3D high-density regime.

Next, in Fig. 4, we show the quasi-2D IBM correlation energy per particle from several ACII functionals in the whole quasi-2D regime (i.e., $0 \leq L/L_{\max} \leq 1$), for $r_s^{2D} = 1, 3$, and 5, respectively. We compare the genISI, genISI2, and UEG-ISI

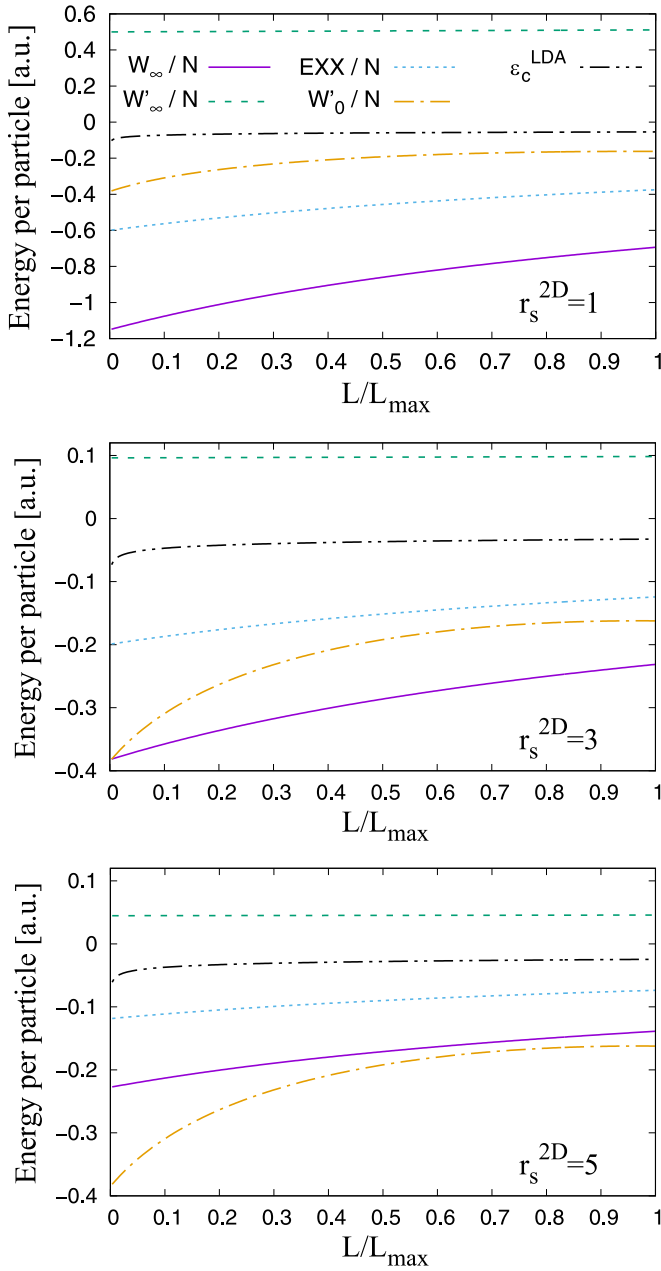


FIG. 3. The quasi-2D IBM ingredients for the ACII functionals. The exact exchange per particle $E_x(L)/N$, $W_\infty(L)/N$ of Eq. (21), $W'_\infty(L)/N$ of Eq. (23), and the $W'_0(L)/N$ for the 2D bulk parameters $r_s^{2D} = 1$ (upper panel), $r_s^{2D} = 3$ (middle panel), and $r_s^{2D} = 5$ (lower panel), respectively.

with the revISI functional, which we have found to be the actual state-of-the-art functional for predicting the 2D correlation energy at $L \rightarrow 0$. We observe that genISI2 performs even better than revISI, being significantly better than genISI. On the other hand, the UEG-ISI underestimates the 2D correlation energy, being accurate only in a mild quasi-2D regime (i.e., $L/L_{\max} \geq 0.6$). Nevertheless, we recall that the quasi-2D IBM is a very difficult test for any XC functional, and for example, the random phase approximation (RPA) performs worse than UEG-ISI (see Fig. 3 of Ref. [72]). On the other hand, the semilocal correlation functional, e.g., PBE [75], cannot de-

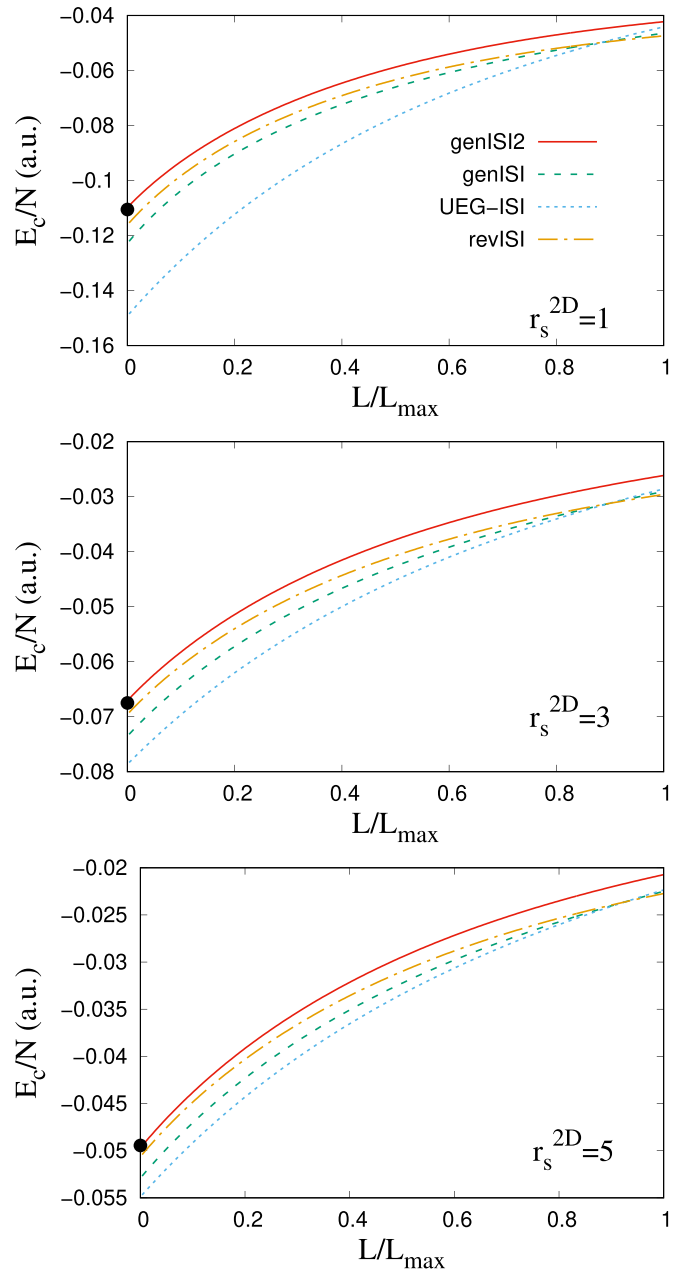


FIG. 4. Correlation energy per particle (ϵ_c) of the IBM quasi-2D electron gas of fixed 2D electron density [$r_s^{2D} = 1$ (upper panel), $r_s^{2D} = 3$ (middle panel), and $r_s^{2D} = 5$ (lower panel), respectively], as a function of the normalized quantum-well thickness L/L_{\max} . The dots at $L = 0$ represent the exact correlation energies of the 2D UEG.

scribe the moderate and strong quasi-2D IBM regimes, being accurate at $L/L_{\max} = 1$ but approaching 0 at $L/L_{\max} = 0$ [45].

B. Two-dimensional uniform electron gas (2D UEG)

We test the ACII functionals for the 2D UEG, where all the ingredients are known and discussed above; $W_0^{2D}/N = -4\frac{\sqrt{2}}{3\pi}\frac{1}{r_s^{2D}}$, $E_c^{GL2-2D}/N = -0.1925$ Ha, $W_\infty^{2D}/N = (\frac{8}{3\pi} - 2)\frac{1}{r_s^{2D}}$, and $W_\infty'^{2D}/N = \frac{1}{2(r_s^{2D})^{3/2}}$.

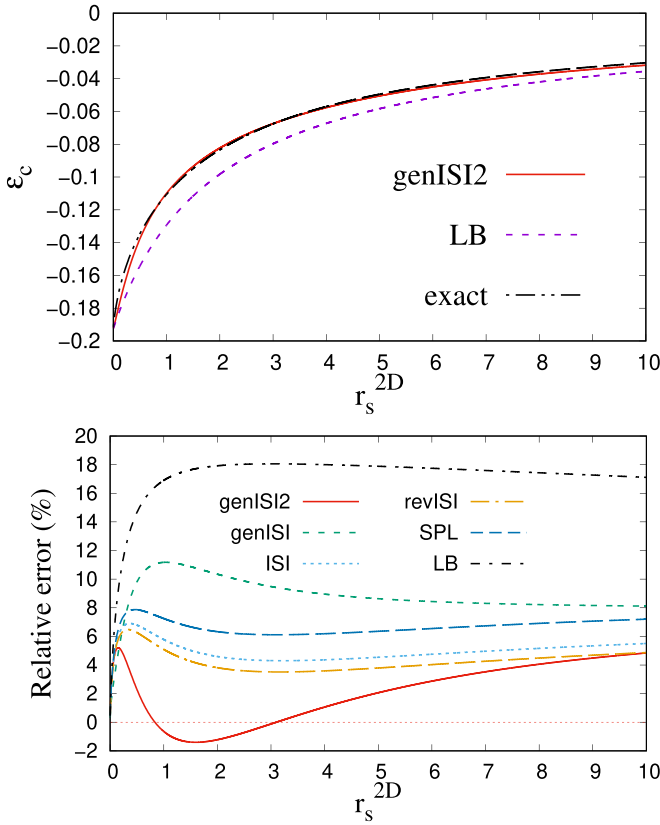


FIG. 5. (Upper panel) 2D UEG correlation energy per particle ϵ_c vs the 2D bulk parameter r_s^{2D} . The exact curve is the 2D LDA correlation energy parametrization of Ref. [65]. (Lower panel) Relative errors (in %) of the correlation energy of the 2D UEG [$100 \times (\text{approx} - \text{exact})/\text{exact}$] obtained from various ACII functionals.

In the upper panel of Fig. 5, we show that genIS12 is remarkably close to the 2D exact LDA correlation energy per particle [65] for any value of the 2D bulk parameter r_s^{2D} , even in the high-density limit. In the lower panel of Fig. 5, we report the relative errors (in %) of the ACII functionals. The best performance is found for genIS12, followed by revISI and ISI, while LB and genIS1 give the worst results.

To better quantify these results, let us consider the following integrated MARE (iMARE):

$$\text{iMARE} = \frac{1}{(10-b)} \int_b^{10} dr_s \frac{|\epsilon_c^{\text{approx}}(r_s) - \epsilon_c^{\text{exact}}(r_s)|}{|\epsilon_c^{\text{exact}}(r_s)|} \times 100, \quad (26)$$

where we take ($b = 0$) for the 2D UEG. We also compute Eq. (26) for the 3D UEG with the choices ($b = 0$) and ($b = 1$). We recall that the considered ACII functionals are not accurate for the 3D UEG in the limit $r_s \rightarrow 0$, where $\epsilon_c^{\text{exact}} \rightarrow 0.031091 \ln(r_s) - 0.0469203$, while $\epsilon_c^{\text{ISI}}, \epsilon_c^{\text{revISI}} \sim 1/\sqrt{r_s}$, $\epsilon_c^{\text{UEG-ISI}} \rightarrow -0.086$. In contrast, SPL and LB functionals perform as $\rightarrow 1/r_s$ not being integrable in the high-density limit. Nevertheless, we note that most bulk metals have $1 \leq r_s \leq 10$. The iMARE values of Eq. (26)

TABLE II. The iMARE of Eq. (26) for the 2D UEG and 3D UEG. Best result is shown in bold style.

	2D UEG		3D UEG	
	$b = 0$	$b = 1$	$b = 1$	$b = 0$
ISI	5.0	45.0	59.4	
revISI	4.3	27.3	37.7	
SPL	6.6	241.5	∞	
LB	17.2	241.5	∞	
UEG-ISI	18.9	0.9	2.4	
genIS1	8.9	0.9	2.4	
genIS12	2.5	0.9	2.4	
PBE	100	0.0	0.0	

for both the 2D and 3D UEG are reported in Table II from the considered ACII functionals. For completeness, we also show the PBE values. For the 2D UEG (considering the limit $L/L_{\text{max}} \rightarrow 0$), the PBE correlation vanishes [70], while for the 3D UEG becomes exact, recovering the Perdew-Wang parametrization of the 3D UEG correlation energy per particle [124].

Thus, we conclude this subsection by noting that the improvement of genIS12 over the genIS1 is substantial for both quasi-2D IBM and 2D UEG and, corroborated with its 3D UEG accurate behavior, can make this functional attractive for various solid-state applications.

C. Finite systems

1. Role of reference orbitals

The genIS12 functional has been parametrized on exact ingredients, reported in Table I. For practical applications, however, such exact values are not known. In Table III, we report accurate results for the harmonium ($\kappa = 1/4$), He, and Ne atoms as obtained from accurate FCI [or CCSD(T)] density (as described in Sec. III C). Our results for W_0 and E_c^{GL2} for the harmonium and He atom reproduce previous exact results from the literature obtained in different ways, see Table I. Data for W_∞ and W'_∞ in Table III have been computed with the hPC functional with the accurate density.

The second row (labelled with ∂_i) of each section of Table III reports the relative derivatives of E_c^{genIS12} with respect to the various ingredients, i.e.,

$$\partial_i = \frac{1}{W_i} \frac{\partial E_c^{\text{genIS12}}}{\partial W_i} \quad (27)$$

where W_i is one of the four ingredients (W_0, W_∞, W'_∞ , and E_c^{GL2}). The E_c^{GL2} ingredient has the largest coefficients, particularly for atomic systems. For those systems, thus the $W'_0 = 2E_c^{\text{GL2}}$ ingredient has a very large impact on the final correlation energy. For this reason, its accurate calculation is much more important than the SCE ingredient.

Then, we compute the ACII ingredients considering different input orbitals and densities (S-VWN [125], PBE, HF, and OEPx), which are routinely available. We can see that the type of input orbitals has a drastic effect on the E_c^{GL2} energy (relative deviations $-38\% \dots +11\%$). In contrast, the

TABLE III. The ACII ingredients for different input densities, in case of the the harmonium ($\kappa = 1/4$), helium, and neon atoms. We used the uncontracted aug-cc-pV6Z basis set, except for harmonium, where a special basis set is utilized [111]. Values of W_∞ and W'_∞ are computed with the hPC functional [48]. The last two columns report the genISI2 correlation energy and the HOMO-LUMO gap. We also report the relative derivatives $[\partial]$, see Eq. (27) for FCI / CCSD(T) densities.

	W_0	W_∞	W'_∞	E_c^{GL2}	$E_c^{genISI2}$	Gap (eV)
Harmonium						
FCI	-0.515	-0.743	0.207	-0.0496	-0.0370	11.47
∂	-15.7%	15.7%	8.4%	18.9%		
S-VWN	-0.511 (-0.8%)	-0.738 (-0.7%)	0.204(-1.4%)	-0.0497(+0.2%)	-0.0371	11.32
PBE	-0.513 (-0.4%)	-0.741 (-0.3%)	0.205(-1.0%)	-0.0498(+0.4%)	-0.0372	11.42
HF	-0.515 (0%)	-0.743 (0%)	0.208(0.5%)	-0.0304(-38%)	-0.0283	20.84
OEPx	-0.515 (0%)	-0.743 (0%)	0.208(0.5%)	-0.0494(-0.4%)	-0.0368	11.45
Helium						
FCI	-1.024	-1.491	0.644	-0.0480	-0.0414	20.40
∂	-6.9%	+6.9%	+2.6%	+27.1%		
S-VWN	-0.998 (-2.5%)	-1.454 (-2.5%)	0.619 (-3.9%)	-0.0533 (+11%)	-0.0440	16.90
PBE	-1.013 (-1.1%)	-1.476 (-1.0%)	0.634 (-1.6%)	-0.0514 (+7.1%)	-0.0431	17.00
HF	-1.026 (+0.2%)	-1.492 (+0.1%)	0.645 (+0.2%)	-0.0366 (-23%)	-0.0345	27.46
OEPx	-1.026 (+0.2%)	-1.492 (+0.1%)	0.646 (+0.3%)	-0.0478 (-0.4%)	-0.0412	20.77
Neon						
CCSD(T)	-12.078	-20.051	23.041	-0.4741	-0.3884	17.12
∂	-2.6%	+2.5%	+0.3%	+29.5%		
S-VWN	-12.008 (-0.6%)	-19.964 (-0.4%)	22.952 (-0.4%)	-0.499 (+5.3%)	-0.403	15.53
PBE	-12.044 (-0.3%)	-20.011 (-0.2%)	23.016 (-0.1%)	-0.491 (+3.6%)	-0.421	15.15
HF	-12.108 (+0.2%)	-20.076 (+0.1%)	23.045 (0%)	-0.367 (-22.6%)	-0.320	27.39
OEPx	-12.104 (+0.2%)	-20.078 (+0.1%)	23.044 (0%)	-0.4631(-2.3%)	-0.3819	18.44

other quantities are not much affected (with a relative deviation of few percent, and often much smaller). In fact, the value of the E_c^{GL2} energy is directly related to the HOMO-LUMO energy gap (last column of Table III), whereas the other ingredients depend only on the ground-state density (matrix), which does not change much. PBE overestimates $|E_c^{GL2}|$, whereas HF largely underestimates it. Similarly, reduced values of $|E_c^{GL2}|$ will be obtained for all global and range-separated hybrid functionals with a HOMO-LUMO gap approaching the many-body one [126,127]. Instead, the ACII functionals require the much smaller KS gap, so that a $|E_c^{GL2}|$ larger than the exact correlation energy is obtained. In fact, the total correlation energy from ACII formulas is always a fraction of the input $|E_c^{GL2}|$ correlation. The best agreement with the reference E_c^{GL2} is obtained using OEPx orbitals, and in fact, OEPx gives an energy gap closer to the reference KS one [48,128].

More sophisticated approaches [48,112] are more computationally demanding or numerically cumbersome. In addition, although a full self-consistent calculation of ACII functionals is possible [48], a more direct assessment of the functionals can be done using the same exact-exchange reference orbitals (i.e., OEPx), resembling the density-corrected DFT [129]. Thus, the calculation of genISI2 correlation energies on OEPx orbitals seems the best choice, considering both the accuracy and the computational cost. Then, for all finite systems, the considered ACII functionals have been evaluated using OEPx orbitals.

If the genISI2 functional is used with very different orbitals (PBE, HF), a proper scaling of the E_c^{GL2} must be used. Otherwise, the results can be quite nonphysical.

2. Harmonium

In Fig. 6, we show the relative errors (in %) given by ACII functionals for harmonium within a broad interval of frequencies $0.03 \leq \omega \leq 1000$. Calculations are done using OEPx orbitals, which gives quite an accurate density in this case [47,48].

In the strongly correlated regime (i.e., $\omega \leq 0.5$), the best result is given by the LB followed by the genISI2 (with

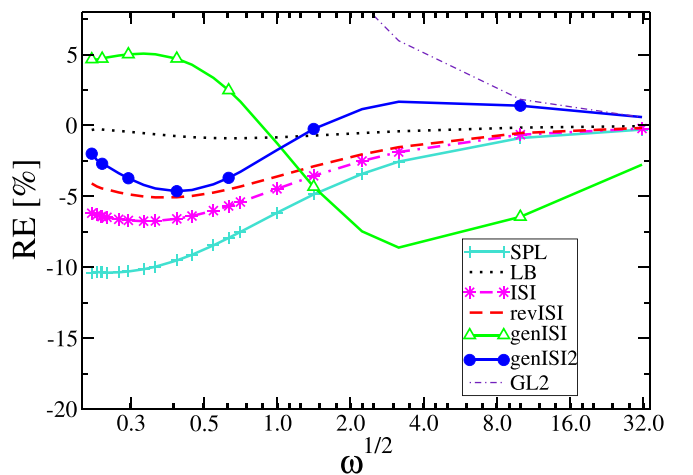


FIG. 6. Relative error on correlation energies of harmonium at various values of ω computed with OEPx orbitals for several ACII functionals using the hPC model for the strong-interaction functionals. The errors have been computed with respect to FCI data obtained in the same basis set [111].

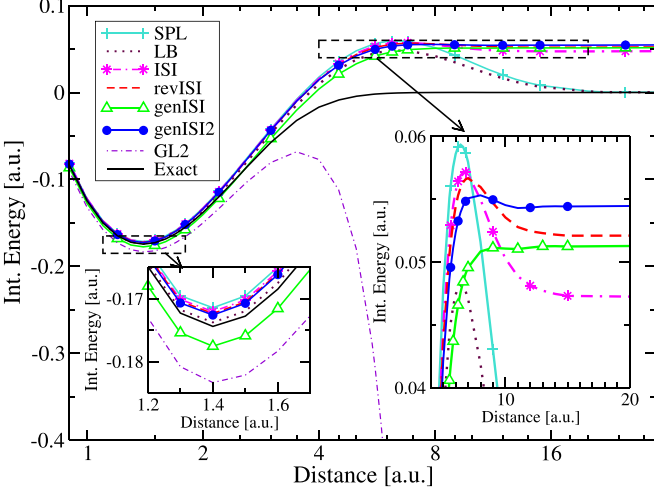


FIG. 7. H_2 dissociation curve computed in a spin-restricted formalism with several ACII functionals, using OEPx orbitals. The exact curve is also reported.

$-2\% \lesssim RE \lesssim -0.5\%$), while the worst is SPL (with the error below 10%). GL2 is very inaccurate in this region. On the other hand, for the tighter bound electrons ($\omega \geq 1$) until the high-density limit ($\omega \gtrsim 100$), the genISI2 gives a similar performance to other methods being much better than genISI, which is the worst.

Overall, the genISI2 (MARE = 2.77%) improves over the genISI (MARE = 4.55%), being better than other functionals, such as SPL (MARE = 7.66%), ISI (MARE = 5.09%), and revISI (MARE = 3.79%). The LB gives the smallest MARE = 0.52%, which is consistent with other predictions [44], and it has been related to a very efficient error cancellation effect in the coupling-constant-averaged energy density for small and large distances.

3. H_2 Dissociation

In Fig. 7, we report the H_2 dissociation curve using a spin-restricted formalism for ISI, revISI, genISI, and genISI2, as well as the FCI (exact) results. We used OEPx orbitals and aug-cc-pV5Z basis-set. Note that, for two-electron systems, OEPx calculation can be done exactly, as the exchange potential is half of the Hartree potential [130]. In addition, the singly excited term vanishes [112]. Figure 7 highlights three important regions:

(i) at equilibrium distance (see inset on the left), all methods are quite accurate. The highest accuracy is obtained from LB, genISI2, ISI, and revISI, while genISI over-binds and SPL under-binds.

(ii) at the dissociation limit, all ISI methods converge to a constant D , in contrast to GL2, which diverges. The constant D can be directly computed as

$$D = E[H_2] - 2E[H] = 2(E[H_{1/2,1/2}] - E[H]), \quad (28)$$

where $E[H_{1/2,1/2}]$ is the total energy of the strongly correlated hydrogen atom [86] with half electron spin-up spin-down occupation. The resulting energies are reported in Table IV. In the limit $E_c^{GL2} = -\infty$, genISI and genISI2 reduce to the same UEG-ISI functional, and thus the same energy ($-0.47239 E_h$)

TABLE IV. Total energy in E_h of $H_{1/2,1/2}$ and the hydrogen atom (H) for different methods. Results for $H_{1/2,1/2}$ are reported with both OEPx and exact orbitals. For H, OEPx orbital is exact. The MARE% is $100(H_{1/2,1/2} - H)/0.5$ at OEPx orbitals.

	$H_{1/2,1/2}$		H	MARE%
	@OEPx	@Exact	@Exact	
OEPx	-0.35769	-0.34373	-0.5	28.5%
PBE	-0.45366	-0.45639	-0.49941	9.1%
r^2 SCAN	-0.44804	-0.45034	-0.5	10.4%
M06	-0.43481	-0.43552	-0.49958	13.0%
ISI	-0.47591	-0.48120	-0.5	4.82%
revISI	-0.47350	-0.47738	-0.5	5.30%
genISI	-0.47239	-0.47536	-0.49840	5.20%
genISI2	-0.47239	-0.47536	-0.5	5.52%
SPL	-0.49994	-0.51676	-0.5	0.01%
LB	-0.49994	-0.51676	-0.5	0.01%
Exact	-0.5	-0.5	-0.5	

is obtained. An almost perfect agreement is obtained with the SPL and LB functionals. We recall that SPL and LB perform identical (as W_∞), in the limit $E_c^{GL2} = -\infty$. However, it should be considered that this is just an error cancellation between the approximated electronic density and the (approximated) hPC SCE model. Using the exact density, in fact, the SPL and LB give a too low energy. The difference between SPL (LB) and the other ACII functionals originates from the W'_∞ contribution, which does not vanish using approximated expressions, such as PC or hPC, see Ref. [48]. The exact W'_∞ is zero for $E[H_{1/2,1/2}]$, and, in this case, all the ACII functionals will be identical to SPL (LB). Table IV also shows that all ACII functionals are more accurate than other conventional functionals, such as PBE, r^2 SCAN [131] and M06 [132]

(iii) in the region around 4–8 a.u. (see right inset), a large repulsive bump emerges in the case of SPL and LB, and also for ISI and revISI. On the other hand, genISI and genISI2 show a much smoother curve. The bump is related to deficiencies of XC energy expression to describe fully the regions where static and dynamic correlation effects interplay. This issue has already been discussed in the literature in different contexts [41,90–92]. We note that proper dissociation for H_2 can be recovered using highly nonlocal [41] forms of AC or by using simple AC formulas [93] with accurate input ingredients for W_∞ and W'_∞ .

In summary, the genISI2 provides a quite accurate description of the H_2 dissociation curve, performing significantly better than genISI near the equilibrium distance, while at large distances between the H atoms, both genISI2 and genISI are similar, recovering the UEG-ISI functional. Their behaviors strongly depend on the quality of the approximations for W_∞ and W'_∞ . However, they yield the exact result when the exact SCE W_∞ and W'_∞ ingredients are used.

4. Molecular systems

First, we show in Table V the total energies (in E_h) for a test-set of five atoms and 11 small molecules, previously used in *ab initio* DFT calculations [112]. Although total energies

TABLE V. Total energies (E_h) for several ACII functionals computed using OEPx orbitals, with respect to CCSD(T) reference data. The last two rows report the MAE (in mE_h) and MARE errors. For comparison, we also report total energies from MP2 and some conventional DFT functionals (PBE, r^2 SCAN and M06, with self-consistent densities). The best results from ACII functionals are boldfaced.

System	CCSD(T)	MP2	PBE	r^2 SCAN	M06	LB	SPL	ISI	revISI	genISI	genISI2
He	-2.9025	-2.8970	-2.8929	-2.9050	-2.9118	-2.9032	-2.9015	-2.9019	-2.9021	-2.9024	-2.9028
Be	-14.6623	-14.6424	-14.6299	-14.6502	-14.6638	-14.6767	-14.6728	-14.6710	-14.6702	-14.6745	-14.6655
Ne	-128.9000	-128.8924	-128.8659	-128.9606	-128.9559	-128.9465	-128.9363	-128.9273	-128.9231	-128.9287	-128.9083
Mg	-199.8282	-199.8157	-199.9539	-200.0831	-200.0648	-199.8690	-199.8657	-199.8656	-199.8656	-199.8637	-199.8663
Ar	-527.4575	-527.4336	-527.3451	-527.5971	-527.5363	-527.5440	-527.5309	-527.5148	-527.5071	-527.5089	-527.4882
HF	-100.3958	-100.3861	-100.3859	-100.4627	-100.4469	-100.4534	-100.4419	-100.4315	-100.4266	-100.4323	-100.4096
CO	-113.2574	-113.2339	-113.2323	-113.3237	-113.2986	-113.3680	-113.3476	-113.3277	-113.3185	-113.3260	-113.2872
H ₂ O	-76.3869	-76.3720	-76.3754	-76.4404	-76.4200	-76.4457	-76.4327	-76.4208	-76.4152	-76.4211	-76.3958
H ₂	-1.1727	-1.1650	-1.1662	-1.1867	-1.1716	-1.1717	-1.1695	-1.1702	-1.1705	-1.1720	-1.1711
He ₂	-5.8051	-5.7939	-5.7859	-5.8098	-5.8238	-5.8040	-5.8008	-5.8017	-5.8021	-5.8018	-5.8038
Cl ₂	-919.7703	-919.7222	-920.0431	-920.4839	-920.3740	-919.9427	-919.9302	-919.9241	-919.9211	-919.9300	-919.9098
N ₂	-109.4763	-109.4562	-109.4507	-109.5365	-109.5040	-109.6093	-109.5861	-109.5611	-109.5497	-109.5548	-109.5134
Ne ₂	-257.8000	-257.7850	-257.7319	-257.9211	-257.9119	-257.8931	-257.8727	-257.8548	-257.8463	-257.8574	-257.8168
HCl	-460.5093	-460.4823	-460.6385	-460.8714	-460.8074	-460.5920	-460.5855	-460.5823	-460.5807	-460.5854	-460.5746
NH ₃	-56.5233	-56.5016	-56.5072	-56.5670	-56.5407	-56.5715	-56.5588	-56.5486	-56.5439	-56.5516	-56.5253
C ₂ H ₆	-79.7641	-79.7145	-79.7270	-79.8288	-79.7821	-79.8343	-79.8124	-79.7988	-79.7923	-79.8106	-79.7630
MAE		19.87	58.46	127.52	100.25	63.60	53.16	43.96	39.66	44.86	24.86
MARE		0.086%	0.111%	0.141%	0.082%	0.056%	0.062%	0.048%	0.041%	0.039%	0.022%

are not very important in practical chemical applications, they are essential observables and are especially useful as indicators of the quality of the ACII interpolation functions.

The genISI2 (with MAE $\approx 25 mE_h$ and MARE $\approx 0.02\%$) gives the best performance among ACII functionals, being almost twice better than revISI (MAE $\approx 40 mE_h$ and MARE $\approx 0.04\%$), which is slightly more accurate than ISI and genISI. These results are followed by SPL (MAE $\approx 53 mE_h$ and MARE $\approx 0.06\%$) and LB functional (MAE $\approx 64 mE_h$ and MARE $\approx 0.06\%$). The MP2 method yields the best MAE (20 mE_h), but the MARE is quite large due to larger inaccuracies for the smaller systems. The worst performance is given by the semilocal r^2 SCAN (MAE $\approx 127 mE_h$ and MARE $\approx 0.14\%$), which largely overestimate the total energies, as also found in Ref. [133]. Results for M06 and PBE are better than r^2 SCAN, but they are 3–5 times worse than genISI2.

We note that the total energy test is important from the theoretical point of view for all functionals based on the MP2 correlation because it can also show if a given functional that is accurate for atomization energies of molecules relies on an error cancellation (e.g., most semilocal GGA and meta-GGA XC functionals).

Next, let us consider the popular AE6 benchmark that is representative for the atomization energies of a large molecular database [134]. Note that we consider the error versus CCSD(T) results in the same basis-set and not versus experimental results. In this way, a more simple and direct comparison can be performed without considering complete-basis-set extrapolation issues. In Table VI, we show the AE6 atomization energies (in kcal/mol) from the ACII functionals. The genISI2 improves over all the other considered functionals, reducing the MAE from ≈ 33 kcal/mol to ≈ 19 kcal/mol. This is a quite significant improvement. However, we should point out that other conventional approaches such as r^2 SCAN and M06 give much lower errors. [We recall again that our

reference is CCSD(T) in the same-basis-set and not the experimental results.] In fact, the calculation of atomization energies with ACII functional based on KS orbitals is still a challenge, such that the genISI2 functional is an important step in this direction.

To better visualize the performance of each functional, we report in Fig. 8 the absolute relative errors (ARE) on total energies versus the ones on atomization energies for the six molecules of the AE6 test. As shown, the genISI2 gives a systematic improvement for all the molecules. Thus, the maximum error on atomization energies is for the S₂ dimer (ARE = 32.9%), followed by the SiO molecule (ARE = 21%), while all the remaining molecules have ARE below 4%. On the other hand, the total energies are remarkably accurate, the worst case being the SiO molecule with ARE = 0.0298%.

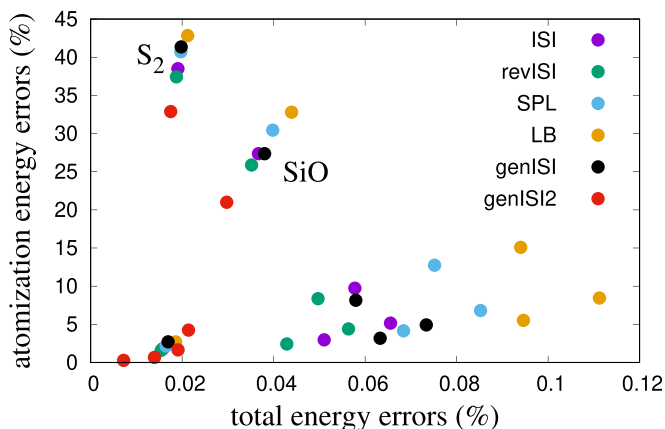


FIG. 8. Absolute relative errors (ARE) on the total energies vs the ARE on atomization energies for the molecules of the AE6 test (SiH₄, SiO, S₂, C₃H₄, C₂H₂O₂, and C₄H₈). We use the CCSD(T) as reference data (see also Table VI).

TABLE VI. Atomization energies (in kcal/mol) of the AE6 test. For ACII functionals OEPx orbitals are used, while for PBE, r²SCAN and M06 self-consistent densities are employed. The last two rows report the error statistics (MAE and MARE) computed with respect to CCSD(T) reference data. The best ACII results are highlighted in bold.

	CCSD(T)	PBE	r ² SCAN	M06	LB	SPL	ISI	revISI	genISI	genISI2
SiH ₄	318.8	311.9	320.0	326.0	327.4	325.7	324.5	323.9	327.4	320.9
SiO	182.0	193.5	185.1	189.4	241.7	237.4	231.8	229.1	231.8	220.2
S ₂	94.3	112.6	109.2	103.5	134.7	132.7	130.6	129.6	133.3	125.3
C ₃ H ₄	690.8	721.4	704.8	705.1	749.1	737.8	726.4	721.2	724.8	702.2
C ₂ H ₂ O ₂	618.1	664.4	635.9	637.0	711.4	696.9	678.3	669.8	668.5	644.3
C ₄ H ₈	1130.5	1168.8	1151.4	1148.1	1192.9	1177.3	1164.1	1158.0	1166.4	1133.6
MAE		25.3	12.0	12.4	53.8	45.6	36.9	32.9	36.3	18.7
MARE		7.2%	4.1%	3.8%	17.9%	16.2%	14.3%	13.4%	14.6%	10.1%

In Table VII, we show the results for the ionization potentials of the 32 systems (atoms and small molecules) reported in Ref. [116]. The best result among ACII group

of approximation is found from genISI2 (MARE = 3.5%, MAE = 0.44 eV), which gives a systematic improvement over the other functionals, providing the best result for 27 systems

TABLE VII. Ionization potentials (in eV) computed from an energy difference obtained for several ACII expressions. For comparison, we also report the PBE, r²SCAN, and M06 ionization potentials; PBE, r²SCAN, and M06 are from self-consistent densities. The last two rows report the error statistics [MAE (eV) and MARE (%)] computed with respect to reference data. The best results from ACII functionals are boldfaced.

	Ref.	PBE	r ² SCAN	M06	LB	SPL	ISI	revISI	genISI	genISI2
Ar	-15.63	-15.70	-15.81	-15.81	-16.15	-16.10	-16.01	-15.97	-15.94	-15.89
Be	-9.31	-9.00	-8.59	-8.94	-9.72	-9.63	-9.58	-9.55	-9.76	-9.38
C ₂ H ₂	-11.43	-11.40	-11.21	-11.17	-12.36	-12.21	-12.01	-11.91	-11.88	-11.64
C ₂ H ₄	-10.63	-10.60	-10.38	-10.35	-11.40	-11.25	-11.07	-10.99	-11.00	-10.72
C ₂ H ₆	-13.01	-11.93	-12.07	-12.25	-12.70	-12.69	-12.70	-12.70	-12.74	-12.71
CH ₂ CF ₂	-10.61	-10.30	-10.27	-10.41	-11.00	-10.93	-10.84	-10.79	-10.78	-10.67
CH ₃ CN	-10.75	-10.42	-10.45	-10.56	-11.94	-11.80	-11.61	-11.52	-11.47	-11.28
CH ₄	-14.37	-13.95	-14.16	-14.08	-14.65	-14.58	-14.51	-14.49	-14.52	-14.37
CHF ₃	-14.59	-13.40	-13.80	-14.20	-15.75	-15.71	-15.67	-15.65	-15.67	-15.60
Cl ₂	-11.45	-11.21	-11.47	-11.49	-11.05	-11.06	-11.07	-11.08	-11.07	-11.10
CO ₂	-13.70	-13.61	-13.64	-13.80	-14.93	-14.80	-14.62	-14.54	-14.49	-14.33
CO	-13.94	-13.82	-13.91	-13.90	-14.62	-14.54	-14.46	-14.42	-14.42	-14.31
CS	-11.27	-11.27	-11.27	-11.22	-14.16	-14.02	-13.82	-13.72	-13.73	-13.45
FCN	-13.65	-13.27	-13.28	-13.33	-15.83	-15.68	-15.46	-15.36	-15.29	-15.11
H ₂ CO	-10.83	-10.69	-10.60	-10.85	-11.70	-11.58	-11.42	-11.35	-11.32	-11.16
H ₂ CS	-9.29	-9.23	-9.16	-9.26	-10.47	-10.39	-10.28	-10.22	-10.22	-10.07
H ₂ O	-12.50	-12.60	-12.42	-12.59	-13.19	-13.08	-12.92	-12.85	-12.83	-12.66
HCCF	-11.50	-11.13	-11.09	-11.16	-12.08	-11.97	-11.82	-11.75	-11.71	-11.57
HCl	-12.59	-12.69	-12.75	-12.70	-13.15	-13.11	-13.07	-13.06	-13.10	-12.98
HCN	-13.90	-13.73	-13.57	-13.69	-15.74	-15.54	-15.26	-15.14	-15.06	-14.80
He	-24.48	-24.47	-24.62	-24.79	-24.54	-24.50	-24.51	-24.52	-24.51	-24.54
He ₂	-24.48	-21.50	-21.30	-22.57	-24.62	-24.60	-24.58	-24.56	-25.17	-24.42
HF	-15.96	-16.11	-15.97	-16.10	-16.68	-16.58	-16.43	-16.37	-16.35	-16.18
Mg	-7.57	-7.61	-7.55	-7.57	-8.03	-8.00	-7.99	-7.98	-8.16	-7.92
N ₂	-15.51	-15.34	-15.61	-15.62	-13.96	-14.11	-14.52	-14.69	-15.00	-14.95
NCCN	-13.51	-13.12	-13.16	-13.18	-13.34	-13.51	-13.94	-14.12	-14.44	-14.43
Ne ₂	-21.34	-18.55	-18.98	-19.71	-22.03	-21.94	-21.81	-21.75	-21.74	-21.59
Ne	-21.47	-21.66	-21.50	-21.72	-22.08	-21.98	-21.86	-21.80	-21.80	-21.64
NH ₃	-10.78	-10.83	-10.67	-10.74	-11.31	-11.20	-11.08	-11.02	-11.02	-10.84
OCS	-11.18	-11.22	-11.31	-11.26	-12.30	-12.22	-12.09	-12.03	-11.99	-11.89
P ₂	-10.66	-10.49	-10.57	-10.62	-10.38	-10.38	-10.38	-10.38	-10.38	-10.37
SiH ₄	-12.78	-12.40	-12.38	-12.61	-13.02	-12.99	-12.97	-12.96	-13.01	-12.91
MAE	0.00	0.40	0.40	0.29	0.80	0.71	0.61	0.57	0.59	0.44
MARE	0.00%	2.54%	2.58%	1.87%	6.45%	5.75%	4.95%	4.59%	4.74%	3.52%

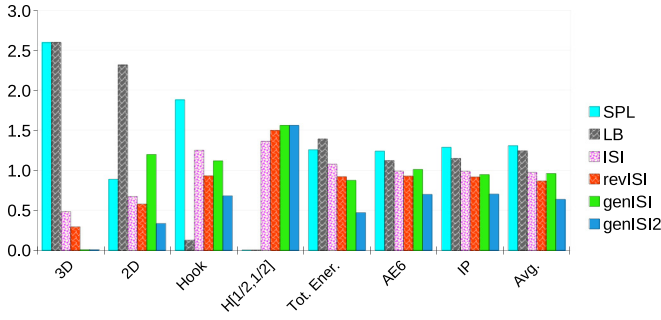


FIG. 9. Bar plot of the normalized MARE for the seven tests and the six ACII functionals considered in this paper. The last section reports the normalized MARE averaged over all tests.

out of 32. After that, ISI, revISI, and genISI give almost similar performances (with $4.6\% \leq \text{MARE} \leq 5\%$ and $0.57 \text{ eV} \leq \text{MAE} \leq 0.61 \text{ eV}$), while SPL and LB have the worst performances, with $\text{MAE} \geq 0.7 \text{ eV}$. We note that genISI2 gives very similar performance to other conventional approximations such as PBE ($\text{MAE} = 0.4 \text{ eV}$; $\text{MARE} = 2.54\%$) or $r^2\text{SCAN}$ ($\text{MAE} = 0.4 \text{ eV}$; $\text{MARE} = 2.58\%$) being only slightly worse than M06 functional ($\text{MAE} = 0.29 \text{ eV}$; $\text{MARE} = 1.87\%$).

V. SUMMARY AND CONCLUSIONS

We have developed an ACII approach, denoted as genISI2, that satisfies the negativity constraint of the correlation energy and the exact conditions for the weak- and strong-interaction limits. When the GL2 correlation diverges, the genISI2 approach recovers the UEG-ISI functional, which is correct for the 3D uniform electron gas. On the other limit, i.e., when the GL2 correlation vanishes, the genISI2 correlation energy also correctly goes to zero, see Eq. (17).

The genISI2 functional is based on two parameters that have been fixed from the correlation energies of small systems, where the ingredients used for the weak- and strong-interaction limits (W_0 , W'_0 , W_∞^{SCE} , and $W_\infty'^{SCE}$) are known (almost) exactly. Such a simple optimization procedure seems powerful and practical because the AC correlation integrand of the genISI2 functional $W_{c,\alpha}$ achieved good accuracy for both the harmonium and Ne atoms, as reported in Fig. 2. Moreover, improved results are obtained for other very different systems, ranging from two-dimensional systems to atomization energies of molecules.

We compared genISI2 with all the currently available ACII functionals. In Fig. 9, we report the normalized MARE,

$$\eta_i^j = \frac{\text{MARE}_i^j}{\frac{1}{6} \sum_j \text{MARE}_i^j}, \quad (29)$$

where MARE_i^j is the MARE of the i th test for functional j . The index j runs over the six ACII functionals considered, and the index i runs over the seven tests considered, namely: 3D UEG (see Table II), 2D UEG (see Table II), harmonium (see Sec. IV C 2), the strongly correlated hydrogen (see Table IV), total energies of atoms and molecules (see Table V), atomization energies (see Table VI), and ionization potential (see Table VII).

The first section of Fig. 9 shows that for the 3D UEG, as also discussed in Ref. [50], SPL and LB are very inaccurate, while revISI and ISI improve significantly. Instead, by construction, genISI and genISI2 are almost exact.

For the quasi-2D IBM, which is one of the most severe tests for XC density functionals [69], we have shown that the genISI2 performs remarkably well in the whole quasi-2D regime, see Sec. IV A. For the true 2D UEG (see the second section of Fig. 9), the genISI2 is the best functional. Such high accuracy for 3D, quasi-2D and 2D uniform electron gases should make it attractive for various electronic calculations of solid-state and condensed-matter physics.

In the case of finite systems, we have shown that great care is required for the calculation of the GL2 correlation energy, being the most important ingredient to obtain the correct correlation energy, which depends strongly on the chosen ground-state orbital. While fully self-consistent calculations are, in principle, possible [48], a more computationally cheaper yet accurate approach is required to investigate large systems. We have shown in Table III that Kohn-Sham OEPx orbitals can be a reliable choice to obtain accurate ingredients for the weak- and strong-interaction limits (W_0 , W'_0 , W_∞ , and

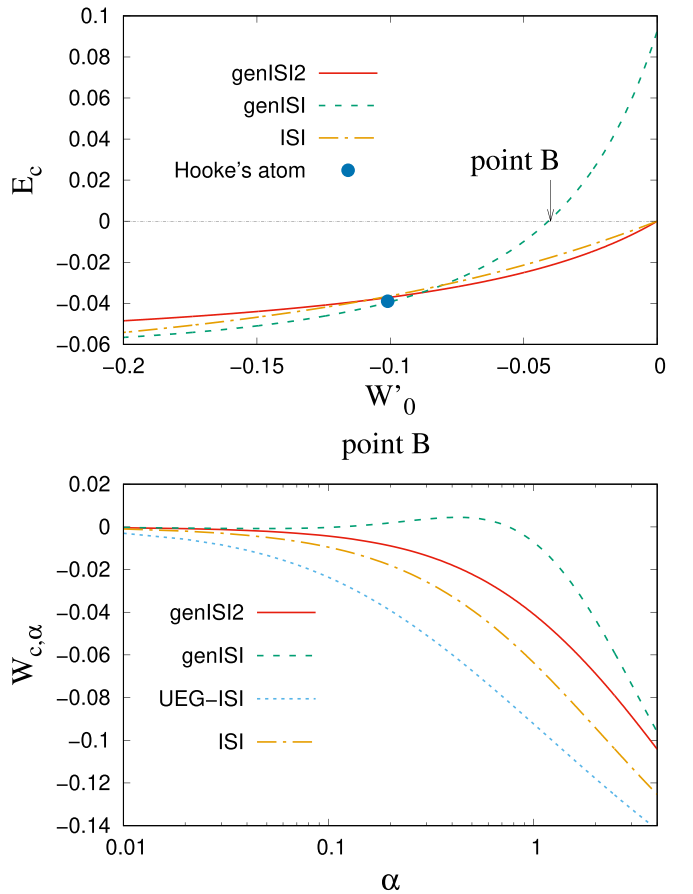


FIG. 10. (Upper panel) The correlation energy E_c (a.u.) vs W'_0 (a.u.) for harmonium ($\kappa = 1/4$), for three ACII functionals. Other ingredients are from Table I. For the harmonium ($\kappa = 1/4$), $W'_0 = -0.101$. (Lower panel) The adiabatic connection correlation integrand $W_{c,\alpha}$ vs α (in log scale), for the point B of the first panel (indicated with an arrow), where $W'_0 = -0.04 \text{ Ha}$.

W'_∞). Thus, all finite-system calculations in this paper have been performed using OEPx orbitals.

For the harmonium (see third section of Fig. 9), genISI2 improves with respect to all ACII functional, except LB, which is almost exact. LB (and also SPL) is almost exact for the H_2 dissociation (see the fourth section of Fig. 9), whereas all the other ACII approaches give similar errors. However, as discussed in Sec. IV C 3, for these strongly correlated electron systems, the accuracy of the results also strongly depends on the accuracy of W_∞ , and W'_∞ (in this paper approximated with hPC) and not only on the ACII interpolation formula. Using the exact SCE for W_∞ , and W'_∞ , all the ACII functionals will be exact.

For atoms and molecular systems, we have observed a systematic improvement of the genISI2 functional with respect to the other ACII approximations for total energies, atomization energies, and ionization potential, see last three sections of Fig. 9. Those are hard tests, despite the fact that the final results are not yet competitive with the most accurate quantum-chemistry methods. Note, in addition, that the genISI2 functional has been parametrized on exact values, whereas for the calculations of real atoms and molecules, approximated quantities are used (i.e., OEPx orbitals instead of exact ones, hPC model data instead of SCE). Thus, further improvement of the results can be expected if this ACII functional is parametrized on those approximated ingredients.

Averaging over all tests, the genISI2 has $\eta = 0.63$, a relevant improvement concerning ISI, revISI, and genISI, which are all above 0.85. We thus expect that genISI2

can have broader applicability and find applications in different areas, ranging from real metal clusters to solid-state systems.

ACKNOWLEDGMENTS

L.A.C. and F.D.S. acknowledge the financial support from ICSC - Centro Nazionale di Ricerca in High Performance Computing, Big Data and Quantum Computing, funded by European Union - NextGenerationEU - PNRR. F.D.S. acknowledges the financial support from PRIN Project No. 2022LM2K5X, Adiabatic Connection for Correlation in Crystals (AC^3) funded by European Union - NextGenerationEU - PNRR. S.Ś. acknowledges the financial support from the National Science Centre, Poland (Grant No. 2021/42/E/ST4/00096).

APPENDIX: THE NEGATIVITY CONDITION OF THE CORRELATION ENERGY

To visualize the negativity condition of the correlation energy, let us fix W_0 , W_∞ , and W'_∞ with the harmonium values (see Table I) and we vary W'_0 (note that for the harmonium $W'_0 = -0.101$). The results are reported in the upper panel of Fig. 10, where we observe that genISI correlation energy becomes positive when $W'_0 \rightarrow 0$, and genISI2 solves this failure. Moreover, as shown in the lower panel of Fig. 10, the correlation integrand $W_{c,\alpha}$ of genISI2 remains smooth, with the correct slope at $\alpha \rightarrow 0$, even for the difficult case when W'_0 is small ($W'_0 = -0.04$), where genISI curve becomes wrongly positive and nonmonotonic.

-
- [1] P. Hohenberg and W. Kohn, Inhomogeneous electron gas, *Phys. Rev.* **136**, B864 (1964).
 - [2] W. Kohn and L. J. Sham, Self-consistent equations including exchange and correlation effects, *Phys. Rev.* **140**, A1133 (1965).
 - [3] K. Burke, Perspective on density functional theory, *J. Chem. Phys.* **136**, 150901 (2012).
 - [4] P. J. Hasnip, K. Refson, M. I. J. Probert, J. R. Yates, S. J. Clark, and C. J. Pickard, Density functional theory in the solid state, *Philos. Trans. R. Soc. A* **372**, 20130270 (2014).
 - [5] F. Giustino, *Materials Modelling Using Density Functional Theory: Properties and Predictions* (Oxford University Press, Oxford, 2014)
 - [6] A. D. Becke, Perspective: Fifty years of density-functional theory in chemical physics, *J. Chem. Phys.* **140**, 18A301 (2014).
 - [7] R. O. Jones, Density functional theory: Its origins, rise to prominence, and future, *Rev. Mod. Phys.* **87**, 897 (2015).
 - [8] W. Kohn, A. D. Becke, and R. G. Parr, Density functional theory of electronic structure, *J. Phys. Chem.* **100**, 12974 (1996).
 - [9] W. Kohn, Nobel lecture: Electronic structure of matter-wave functions and density functionals, *Rev. Mod. Phys.* **71**, 1253 (1999).
 - [10] D. C. Langreth and J. P. Perdew, The exchange-correlation energy of a metallic surface, *Solid State Commun.* **17**, 1425 (1975).
 - [11] O. Gunnarsson and B. I. Lundqvist, Exchange and correlation in atoms, molecules, and solids by the spin-density-functional formalism, *Phys. Rev. B* **13**, 4274 (1976).
 - [12] A. Savin, F. Colonna, and R. Pollet, Adiabatic connection approach to density functional theory of electronic systems, *Int. J. Quantum Chem.* **93**, 166 (2003).
 - [13] A. J. Cohen, P. Mori-Sánchez, and W. Yang, Assessment and formal properties of exchange-correlation functionals constructed from the adiabatic connection, *J. Chem. Phys.* **127**, 034101 (2007).
 - [14] M. Ernzerhof, Construction of the adiabatic connection, *Chem. Phys. Lett.* **263**, 499 (1996).
 - [15] K. Burke, M. Ernzerhof, and J. P. Perdew, The adiabatic connection method: A non-empirical hybrid, *Chem. Phys. Lett.* **265**, 115 (1997).
 - [16] F. Colonna and A. Savin, Correlation energies for some two- and four-electron systems along the adiabatic connection in density functional theory, *J. Chem. Phys.* **110**, 2828 (1999).
 - [17] A. D. Becke, Density-functional thermochemistry. III. The role of exact exchange, *J. Chem. Phys.* **98**, 5648 (1993).
 - [18] C. Adamo and V. Barone, Exchange functionals with improved long-range behavior and adiabatic connection methods without adjustable parameters: The *m*PW and *m*PW1PW models, *J. Chem. Phys.* **108**, 664 (1998).
 - [19] S. Śmiga and L. A. Constantin, Unveiling the physics behind hybrid functionals, *J. Phys. Chem. A* **124**, 5606 (2020).

- [20] J. P. Perdew and K. Schmidt, Jacob's ladder of density functional approximations for the exchange-correlation energy, *AIP Conf. Proc.* **577**, 1 (2001).
- [21] A. Heßelmann and A. Görling, Random-phase approximation correlation methods for molecules and solids, *Mol. Phys.* **109**, 2473 (2011).
- [22] H. Eshuis, J. E. Bates, and F. Furche, Electron correlation methods based on the random phase approximation, *Theor. Chem. Acc.* **131**, 1084 (2012).
- [23] G. P. Chen, V. K. Voora, M. M. Agee, S. G. Balasubramani, and F. Furche, Random-phase approximation methods, *Annu. Rev. Phys. Chem.* **68**, 421 (2017).
- [24] L. Goerigk and S. Grimme, Double-hybrid density functionals, *WIRE Comput. Mol. Sci.* **4**, 576 (2014).
- [25] M. Seidl, J. P. Perdew, and M. Levy, Strictly correlated electrons in density-functional theory, *Phys. Rev. A* **59**, 51 (1999).
- [26] M. Seidl, J. P. Perdew, and S. Kurth, Simulation of all-order density-functional perturbation theory, using the second order and the strong-correlation limit, *Phys. Rev. Lett.* **84**, 5070 (2000).
- [27] M. Seidl, J. P. Perdew, and S. Kurth, Density functionals for the strong-interaction limit, *Phys. Rev. A* **62**, 012502 (2000).
- [28] J. P. Perdew, S. Kurth, and M. Seidl, Exploring the adiabatic connection between weak-and strong-interaction limits in density functional theory, *Int. J. Mod. Phys. B* **15**, 1672 (2001).
- [29] R. Magyar, W. Terilla, and K. Burke, Accurate adiabatic connection curve beyond the physical interaction strength, *J. Chem. Phys.* **119**, 696 (2003).
- [30] P. Gori-Giorgi, G. Vignale, and M. Seidl, Electronic zero-point oscillations in the strong-interaction limit of density functional theory, *J. Chem. Theory Comput.* **5**, 743 (2009).
- [31] Z.-F. Liu and K. Burke, Adiabatic connection in the low-density limit, *Phys. Rev. A* **79**, 064503 (2009).
- [32] Z.-F. Liu and K. Burke, Adiabatic connection for strictly correlated electrons, *J. Chem. Phys.* **131**, 124124 (2009).
- [33] J. Sun, Extension to negative values of the coupling constant of adiabatic connection for interaction-strength interpolation, *J. Chem. Theory Comput.* **5**, 708 (2009).
- [34] M. Seidl and P. Gori-Giorgi, Adiabatic connection at negative coupling strengths, *Phys. Rev. A* **81**, 012508 (2010).
- [35] P. Gori-Giorgi and M. Seidl, Density functional theory for strongly-interacting electrons: Perspectives for physics and chemistry, *Phys. Chem. Chem. Phys.* **12**, 14405 (2010).
- [36] A. Mirtschink, M. Seidl, and P. Gori-Giorgi, Energy densities in the strong-interaction limit of density functional theory, *J. Chem. Theory Comput.* **8**, 3097 (2012).
- [37] Y. Zhou, H. Bahmann, and M. Ernzerhof, Construction of exchange-correlation functionals through interpolation between the non-interacting and the strong-correlation limit, *J. Chem. Phys.* **143**, 124103 (2015).
- [38] S. Vuckovic, T. J. Irons, A. Savin, A. M. Teale, and P. Gori-Giorgi, Exchange-correlation functionals via local interpolation along the adiabatic connection, *J. Chem. Theory Comput.* **12**, 2598 (2016).
- [39] E. Fabiano, P. Gori-Giorgi, M. Seidl, and F. Della Sala, Interaction-strength interpolation method for main-group chemistry: Benchmarking, limitations, and perspectives, *J. Chem. Theory Comput.* **12**, 4885 (2016).
- [40] S. Vuckovic, T. J. Irons, L. O. Wagner, A. M. Teale, and P. Gori-Giorgi, Interpolated energy densities, correlation indicators and lower bounds from approximations to the strong coupling limit of DFT, *Phys. Chem. Chem. Phys.* **19**, 6169 (2017).
- [41] S. Vuckovic and P. Gori-Giorgi, Simple fully nonlocal density functionals for electronic repulsion energy, *J. Phys. Chem. Lett.* **8**, 2799 (2017).
- [42] S. Giarrusso, P. Gori-Giorgi, F. Della Sala, and E. Fabiano, Assessment of interaction-strength interpolation formulas for gold and silver clusters, *J. Chem. Phys.* **148**, 134106 (2018).
- [43] S. Vuckovic, P. Gori-Giorgi, F. Della Sala, and E. Fabiano, Restoring size consistency of approximate functionals constructed from the adiabatic connection, *J. Phys. Chem. Lett.* **9**, 3137 (2018).
- [44] D. P. Kooi and P. Gori-Giorgi, Local and global interpolations along the adiabatic connection of DFT: A study at different correlation regimes, *Theor. Chem. Acc.* **137**, 166 (2018).
- [45] L. A. Constantin, Correlation energy functionals from adiabatic connection formalism, *Phys. Rev. B* **99**, 085117 (2019).
- [46] E. Fabiano, S. Śmiga, S. Giarrusso, T. J. Daas, F. Della Sala, I. Grabowski, and P. Gori-Giorgi, Investigation of the exchange-correlation potentials of functionals based on the adiabatic connection interpolation, *J. Chem. Theory Comput.* **15**, 1006 (2019).
- [47] S. Śmiga and L. A. Constantin, Modified interaction-strength interpolation method as an important step toward self-consistent calculations, *J. Chem. Theory Comput.* **16**, 4983 (2020).
- [48] S. Śmiga, F. Della Sala, P. Gori-Giorgi, and E. Fabiano, Self-consistent implementation of Kohn-Sham adiabatic connection models with improved treatment of the strong-interaction limit, *J. Chem. Theory Comput.* **18**, 5936 (2022).
- [49] S. Vuckovic, A. Gerolin, T. J. Daas, H. Bahmann, G. Friesecke, and P. Gori-Giorgi, Density functionals based on the mathematical structure of the strong-interaction limit of DFT, *WIRE Comput. Mol. Sci.* **13**, e1634 (2023).
- [50] L. A. Constantin, S. Jana, S. Śmiga, and F. Della Sala, Adiabatic connection interaction strength interpolation method made accurate for the uniform electron gas, *J. Chem. Phys.* **159**, 244111 (2023).
- [51] S. Jana, S. Śmiga, L. A. Constantin, and P. Samal, Semilocal meta-GGA exchange-correlation approximation from adiabatic connection formalism: Extent and limitations, *J. Phys. Chem. A* **127**, 8685 (2023).
- [52] A. Görling and M. Levy, Correlation-energy functional and its high-density limit obtained from a coupling-constant perturbation expansion, *Phys. Rev. B* **47**, 13105 (1993).
- [53] S. Jana, S. Śmiga, L. A. Constantin, and P. Samal, Generalizing double-hybrid density functionals: Impact of higher-order perturbation terms, *J. Chem. Theory Comput.* **16**, 7413 (2020).
- [54] A. Görling and M. Levy, Exact Kohn-Sham scheme based on perturbation theory, *Phys. Rev. A* **50**, 196 (1994).
- [55] A. Görling and M. Levy, Hardness of molecules and the band gap of solids within the Kohn-Sham formalism: A perturbation-scaling approach, *Phys. Rev. A* **52**, 4493 (1995).
- [56] P. Gori-Giorgi, M. Seidl, and G. Vignale, Density-functional theory for strongly interacting electrons, *Phys. Rev. Lett.* **103**, 166402 (2009).
- [57] F. Malet and P. Gori-Giorgi, Strong correlation in Kohn-Sham density functional theory, *Phys. Rev. Lett.* **109**, 246402 (2012).

- [58] G. Friesecke, A. Gerolin, and P. Gori-Giorgi, The strong-interaction limit of density functional theory, in *Density Functional Theory: Modeling, Mathematical Analysis, Computational Methods, and Applications*, edited by E. Cancès and G. Friesecke (Springer International Publishing, Cham, 2023), pp. 183–266.
- [59] M. Seidl, S. Giarrusso, S. Vuckovic, E. Fabiano, and P. Gori-Giorgi, Communication: Strong-interaction limit of an adiabatic connection in Hartree-Fock theory, *J. Chem. Phys.* **149**, 241101 (2018).
- [60] T. J. Daas, J. Grossi, S. Vuckovic, Z. H. Musslimani, D. P. Kooi, M. Seidl, K. J. H. Giesbertz, and P. Gori-Giorgi, Large coupling-strength expansion of the Møller–Plesset adiabatic connection: From paradigmatic cases to variational expressions for the leading terms, *J. Chem. Phys.* **153**, 214112 (2020).
- [61] T. J. Daas, E. Fabiano, F. Della Sala, P. Gori-Giorgi, and S. Vuckovic, Noncovalent interactions from models for the Møller–Plesset adiabatic connection, *J. Phys. Chem. Lett.* **12**, 4867 (2021).
- [62] T. J. Daas, D. P. Kooi, A. J. A. F. Grooteman, M. Seidl, and P. Gori-Giorgi, Gradient expansions for the large-coupling strength limit of the Møller–Plesset adiabatic connection, *J. Chem. Theory Comput.* **18**, 1584 (2022).
- [63] K. J. Daas, D. P. Kooi, N. C. Peters, E. Fabiano, F. Della Sala, P. Gori-Giorgi, and S. Vuckovic, Regularized and opposite spin-scaled functionals from Møller–Plesset adiabatic connection—higher accuracy at lower cost, *J. Phys. Chem. Lett.* **14**, 8448 (2023).
- [64] Y. J. Franzke, C. Holzer, J. H. Andersen, T. Begušić, F. Bruder, S. Coriani, F. Della Sala, E. Fabiano, D. A. Fedotov, S. Fürtst *et al.*, Turbomole: Today and tomorrow, *J. Chem. Theory Comput.* **19**, 6859 (2023).
- [65] C. Attaccalite, S. Moroni, P. Gori-Giorgi, and G. B. Bachelet, Correlation energy and spin polarization in the 2D electron gas, *Phys. Rev. Lett.* **88**, 256601 (2002).
- [66] H. Saarikoski, E. Räsänen, S. Siljamäki, A. Harju, M. J. Puska, and R. M. Nieminen, Testing of two-dimensional local approximations in the current-spin and spin-density-functional theories, *Phys. Rev. B* **67**, 205327 (2003).
- [67] J. F. Dobson, Inhomogeneous STLS theory and TDCDFT, *Phys. Chem. Chem. Phys.* **11**, 4528 (2009).
- [68] J. F. Dobson, J. Wang, and T. Gould, Correlation energies of inhomogeneous many-electron systems, *Phys. Rev. B* **66**, 081108(R) (2002).
- [69] L. Pollack and J. Perdew, Evaluating density functional performance for the quasi-two-dimensional electron gas, *J. Phys.: Condens. Matter* **12**, 1239 (2000).
- [70] L. Chiodo, L. A. Constantin, E. Fabiano, and F. Della Sala, Nonuniform scaling applied to surface energies of transition metals, *Phys. Rev. Lett.* **108**, 126402 (2012).
- [71] S. Karimi and C. A. Ullrich, Three-to two-dimensional crossover in time-dependent density-functional theory, *Phys. Rev. B* **90**, 245304 (2014).
- [72] L. A. Constantin, Simple effective interaction for dimensional crossover, *Phys. Rev. B* **93**, 121104(R) (2016).
- [73] A. D. Kaplan, K. Wagle, and J. P. Perdew, Collapse of the electron gas from three to two dimensions in Kohn–Sham density functional theory, *Phys. Rev. B* **98**, 085147 (2018).
- [74] C. M. Horowitz, C. R. Proetto, and J. M. Pitarke, Construction of a semilocal exchange density functional from a three-dimensional electron gas collapsing to two dimensions, *Phys. Rev. B* **108**, 115119 (2023).
- [75] J. P. Perdew, K. Burke, and Y. Wang, Generalized gradient approximation for the exchange–correlation hole of a many-electron system, *Phys. Rev. B* **54**, 16533 (1996).
- [76] J. Tao, J. P. Perdew, V. N. Staroverov, and G. E. Scuseria, Climbing the density functional ladder: Nonempirical meta-generalized gradient approximation designed for molecules and solids, *Phys. Rev. Lett.* **91**, 146401 (2003).
- [77] M. Taut, Two electrons in a homogeneous magnetic field: Particular analytical solutions, *J. Phys. A: Math. Gen.* **27**, 1045 (1994).
- [78] J. P. Coe, A. Sudbery, and I. D’amico, Entanglement and density-functional theory: Testing approximations on Hooke’s atom, *Phys. Rev. B* **77**, 205122 (2008).
- [79] E. V. Ludeña, D. Gómez, V. Karasiev, and P. Nieto, Exact analytic total energy functional for Hooke’s atom generated by local-scaling transformations, *Int. J. Quantum Chem.* **99**, 297 (2004).
- [80] C. Liang, Z. Ping, Y. Tao, and P. Xiao-Yin, Hooke’s atom in an arbitrary external electric field: Analytical solutions of two-electron problem by path integral approach, *Commun. Theor. Phys.* **55**, 565 (2011).
- [81] D. P. O’Neill and P. M. W. Gill, Wave functions and two-electron probability distributions of the Hooke’s-law atom and helium, *Phys. Rev. A* **68**, 022505 (2003).
- [82] P. Gori-Giorgi and A. Savin, Study of the discontinuity of the exchange–correlation potential in an exactly soluble case, *Int. J. Quantum Chem.* **109**, 2410 (2009).
- [83] K.-C. Lam, F. G. Cruz, and K. Burke, Virial exchange–correlation energy density in Hooke’s atom, *Int. J. Quantum Chem.* **69**, 533 (1998).
- [84] K. Burke, F. G. Cruz, and K.-C. Lam, Unambiguous exchange–correlation energy density, *J. Chem. Phys.* **109**, 8161 (1998).
- [85] P. Gill and D. P. O’Neill, Electron correlation in Hooke’s law atom in the high-density limit, *J. Chem. Phys.* **122**, 094110 (2005).
- [86] A. J. Cohen, P. Mori-Sánchez, and W. Yang, Fractional spins and static correlation error in density functional theory, *J. Chem. Phys.* **129**, 121104 (2008).
- [87] P. Mori-Sánchez, A. J. Cohen, and W. Yang, Discontinuous nature of the exchange–correlation functional in strongly correlated systems, *Phys. Rev. Lett.* **102**, 066403 (2009).
- [88] A. J. Cohen, P. Mori-Sánchez, and W. Yang, Second-order perturbation theory with fractional charges and fractional spins, *J. Chem. Theory Comput.* **5**, 786 (2009).
- [89] B. G. Janesko, E. Proynov, J. Kong, G. Scalmani, and M. J. Frisch, Practical density functionals beyond the overdelocalization–underbinding zero-sum game, *J. Phys. Chem. Lett.* **8**, 4314 (2017).
- [90] M. Fuchs, Y.-M. Niquet, X. Gonze, and K. Burke, Describing static correlation in bond dissociation by Kohn–Sham density functional theory, *J. Chem. Phys.* **122**, 094116 (2005).
- [91] I. Y. Zhang, P. Rinke, J. P. Perdew, and M. Scheffler, Towards efficient orbital-dependent density functionals for weak and strong correlation, *Phys. Rev. Lett.* **117**, 133002 (2016).
- [92] W. Ai, W.-H. Fang, and N. Q. Su, Functional-based description of electronic dynamic and strong correlation: Old issues and new insights, *J. Phys. Chem. Lett.* **13**, 1744 (2022).

- [93] M. J. G. Peach, A. M. Miller, A. M. Teale, and D. J. Tozer, Adiabatic connection forms in density functional theory: H2 and the He isoelectronic series, *J. Chem. Phys.* **129**, 064105 (2008).
- [94] A. Teale, S. Coriani, and T. Helgaker, Accurate calculation and modeling of the adiabatic connection in density functional theory, *J. Chem. Phys.* **132**, 164115 (2010).
- [95] I. Y. Zhang and X. Xu, On the top rung of Jacob's ladder of density functional theory: Toward resolving the dilemma of SIE and NCE, *WIREs Comp. Mol. Sci.* **11**, e1490 (2021).
- [96] J. Kirkpatrick, B. McMorro, D. H. P. Turban, A. L. Gaunt, J. S. Spencer, A. G. D. G. Matthews, A. Obika, L. Thiry, M. Fortunato, D. Pfau *et al.*, Pushing the frontiers of density functionals by solving the fractional electron problem, *Science* **374**, 1385 (2021).
- [97] W. Kohn, Discontinuity of the exchange-correlation potential from a density-functional viewpoint, *Phys. Rev. B* **33**, 4331 (1986).
- [98] W. Kohn, Effective mass theory in solids from a many-particle standpoint, *Phys. Rev.* **105**, 509 (1957).
- [99] J. Rey and A. Savin, Virtual space level shifting and correlation energies, *Int. J. Quantum Chem.* **69**, 581 (1998).
- [100] E. Fabiano, P. E. Trevisanutto, A. Terentjevs, and L. A. Constantin, Generalized gradient approximation correlation energy functionals based on the uniform electron gas with gap model, *J. Chem. Theory Comput.* **10**, 2016 (2014).
- [101] S. Ivanov, R. Lopez-Boada, A. Görling, and M. Levy, Closed-form expression relating the second-order component of the density functional theory correlation energy to its functional derivative, *J. Chem. Phys.* **109**, 6280 (1998).
- [102] P. Gori-Giorgi (private communication).
- [103] M. Seidl, P. Gori-Giorgi, and A. Savin, Strictly correlated electrons in density-functional theory: A general formulation with applications to spherical densities, *Phys. Rev. A* **75**, 042511 (2007).
- [104] O. Betbeder-Matibet, M. Combescot, and C. Tanguy, Quasi-two-dimensional electron gas: Exchange and correlation energies, *Phys. Rev. B* **53**, 12929 (1996).
- [105] J. P. Perdew, J. Tao, V. N. Staroverov, and G. E. Scuseria, Meta-generalized gradient approximation: Explanation of a realistic nonempirical density functional, *J. Chem. Phys.* **120**, 6898 (2004).
- [106] J. F. Stanton, J. Gauss, J. D. Watts, M. Nooijen, N. Oliphant, S. A. Perera, P. Szalay, W. J. Lauderdale, S. Kucharski, S. Gwaltney, S. Beck, A. Balková, D. E. Bernholdt, K. K. Baeck, P. Rozyczko, H. Sekino, C. Hober, and R. J. Bartlett, Integral packages included are VMOL (J. Almlöf and P.R. Taylor); VPROPS (P. Taylor) ABACUS; (T. Helgaker, H.J. Aa. Jensen, P. Jörgensen, J. Olsen, and P.R. Taylor), *ACES II* (Quantum Theory Project, Gainesville, Florida, 2007).
- [107] S. Śmiga, O. Franck, B. Mussard, A. Buksztel, I. Grabowski, E. Luppi, and J. Toulouse, Self-consistent double-hybrid density-functional theory using the optimized-effective-potential method, *J. Chem. Phys.* **145**, 144102 (2016).
- [108] S. Śmiga, I. Grabowski, M. Witkowski, B. Mussard, and J. Toulouse, Self-consistent range-separated density-functional theory with second-order perturbative correction via the optimized-effective-potential method, *J. Chem. Theory Comput.* **16**, 211 (2020).
- [109] S. Ivanov, S. Hirata, and R. J. Bartlett, Exact exchange treatment for molecules in finite-basis-set Kohn-Sham theory, *Phys. Rev. Lett.* **83**, 5455 (1999).
- [110] N. R. Kestner and O. Sinanoğlu, Study of electron correlation in helium-like systems using an exactly soluble model, *Phys. Rev.* **128**, 2687 (1962).
- [111] E. Matito, J. Cioslowski, and S. F. Vyboishchikov, Properties of harmonium atoms from FCI calculations: Calibration and benchmarks for the ground state of the two-electron species, *Phys. Chem. Chem. Phys.* **12**, 6712 (2010).
- [112] I. Grabowski, E. Fabiano, A. M. Teale, S. Śmiga, A. Buksztel, and F. Della Sala, Orbital-dependent second-order scaled-opposite-spin correlation functionals in the optimized effective potential method, *J. Chem. Phys.* **141**, 024113 (2014).
- [113] B. J. Lynch and D. G. Truhlar, Small representative benchmarks for thermochemical calculations, *J. Phys. Chem. A* **107**, 8996 (2003).
- [114] R. Haunschild and W. Klopper, Theoretical reference values for the AE6 and BH6 test sets from explicitly correlated coupled-cluster theory, *Theor. Chem. Acc.* **131**, 1112 (2012).
- [115] T. H. Dunning, Gaussian basis sets for use in correlated molecular calculations. I. The atoms boron through neon and hydrogen, *J. Chem. Phys.* **90**, 1007 (1989).
- [116] S. Śmiga, F. Della Sala, A. Buksztel, I. Grabowski, and E. Fabiano, Accurate Kohn-Sham ionization potentials from scaled-opposite-spin second-order optimized effective potential methods, *J. Comput. Chem.* **37**, 2081 (2016).
- [117] S. Śmiga and I. Grabowski, Spin-component-scaled Δ MP2 parametrization: Toward a simple and reliable method for ionization energies, *J. Chem. Theory Comput.* **14**, 4780 (2018).
- [118] K. Raghavachari, G. W. Trucks, J. A. Pople, and M. Head-Gordon, A fifth-order perturbation comparison of electron correlation theories, *Chem. Phys. Lett.* **157**, 479 (1989).
- [119] Q. Wu and W. Yang, A direct optimization method for calculating density functionals and exchange-correlation potentials from electron densities, *J. Chem. Phys.* **118**, 2498 (2003).
- [120] Q. Sun, X. Zhang, S. Banerjee, P. Bao, M. Barbry, N. S. Blunt, N. A. Bogdanov, G. H. Booth, J. Chen, Z.-H. Cui *et al.*, Recent developments in the PySCF program package, *J. Chem. Phys.* **153**, 024109 (2020).
- [121] S. Nam, R. J. McCarty, H. Park, and E. Sim, Ks-pies: Kohn-Sham inversion toolkit, *J. Chem. Phys.* **154**, 124122 (2021).
- [122] T. Heaton-Burgess, F. A. Bulat, and W. Yang, Optimized effective potentials in finite basis sets, *Phys. Rev. Lett.* **98**, 256401 (2007).
- [123] T. van Mourik, A. K. Wilson, and T. H. Dunning, Jr, Benchmark calculations with correlated molecular wavefunctions. XIII. potential energy curves for He2, Ne2 and Ar2 using correlation consistent basis sets through augmented sextuple zeta, *Mol. Phys.* **96**, 529 (1999).
- [124] J. P. Perdew and Y. Wang, Accurate and simple analytic representation of the electron-gas correlation energy, *Phys. Rev. B* **45**, 13244 (1992).
- [125] S. H. Vosko, L. Wilk, and M. Nusair, Accurate spin-dependent electron liquid correlation energies for local spin density calculations: A critical analysis, *Can. J. Phys.* **58**, 1200 (1980).
- [126] R. Baer, E. Livshits, and U. Salzner, Tuned range-separated hybrids in density functional theory, *Annu. Rev. Phys. Chem.* **61**, 85 (2010).

- [127] L. Kronik, T. Stein, S. Refaely-Abramson, and R. Baer, Excitation gaps of finite-sized systems from optimally tuned range-separated hybrid functionals, *J. Chem. Theory Comput.* **8**, 1515 (2012).
- [128] E. Fabiano and F. Della Sala, Localized exchange-correlation potential from second-order self-energy for accurate Kohn-Sham energy gap, *J. Chem. Phys.* **126**, 214102 (2007).
- [129] E. Sim, S. Song, and K. Burke, Quantifying density errors in DFT, *J. Phys. Chem. Lett.* **9**, 6385 (2018).
- [130] M. Weimer, F. Della Sala, and A. Görling, Multiconfiguration optimized effective potential method for a density-functional treatment of static correlation, *J. Chem. Phys.* **128**, 144109 (2008).
- [131] J. W. Furness, A. D. Kaplan, J. Ning, J. P. Perdew, and J. Sun, Accurate and numerically efficient r2SCAN meta-generalized gradient approximation, *J. Phys. Chem. Lett.* **11**, 8208 (2020).
- [132] Y. Zhao and D. G. Truhlar, The m06 suite of density functionals for main group thermochemistry, thermochemical kinetics, noncovalent interactions, excited states, and transition elements: Two new functionals and systematic testing of four m06-class functionals and 12 other functionals, *Theo. Chem. Acc.* **120**, 215 (2008).
- [133] S. Jana, K. Sharma, and P. Samal, Improving the performance of Tao–Mo non-empirical density functional with broader applicability in quantum chemistry and materials science, *J. Phys. Chem. A* **123**, 6356 (2019).
- [134] B. J. Lynch and D. G. Truhlar, Robust and affordable multi-coefficient methods for thermochemistry and thermochemical kinetics: The MCCM/3 suite and SAC/3, *J. Phys. Chem. A* **107**, 3898 (2003).